Theory of optical suppression of ultracold-collision rates by polarized light

Reginaldo Napolitano
Instituto de Física de São Carlos, Universidade de São Paulo, São Carlos, São Paulo 13560-970, Brazil

John Weiner
Department of Chemistry and Biochemistry, University of Maryland, College Park, Maryland 20742

Paul S. Julienne
Molecular Physics Division, National Institute of Standards and Technology, Gaithersburg, Maryland 20899
(Received 30 May 1996)

We have developed a full three-dimensional quantum scattering approach to optical suppression of ultracold-collision rates. These calculations are carried out assuming colliding atoms without fine or hyperfine structure, which have a $^1S \rightarrow {}^1P$ transition. The three-dimensional model predicts that the optical suppression of ultracold-collision rates saturates with light intensity much more slowly than predicted by two-level curve-crossing models. Circularly polarized light is significantly more effective for optical suppression, and causes less increase in atomic kinetic energy due to excited-state production than linearly polarized light. The suppressor optical field can also cause orders of magnitude increases in ground-state elastic-scattering rates. [S1050-2947(97)06701-2]

PACS number(s): 32.80.Pj, 33.80.Ps, 34.50.Rk, 34.80.Qb

I. INTRODUCTION

The quest for achieving Bose-Einstein condensation is a major motivation to investigate the nature of ultracold collisions [1–4]. Such a phase transition is predicted to occur when the thermal de Broglie wavelength of an assembly of atoms becomes comparable to the average interatomic distance [5,6]; but inelastic collision processes restrict the density of trapped atoms [7]. These inelastic processes lead to loss of atoms from magneto-optical [8–16], far-off-resonance [17,18], or purely magnetic [19–21] traps. Recently, however, optical shielding of short-range collision processes in ensembles of cold atoms has been demonstrated experimentally [12,22–27] and interpreted theoretically [28]. This phenomenon presents the prospect of appreciably reducing occurrence of collisions that lead to loss of trapped atoms and strongly enhancing the ground-state elastic-scattering rate.

The essential phenomenon underlying optical shielding requires the existence of a long-range, excited molecular repulsive potential curve commonly arising from the dipole-dipole interaction between two identical atoms exchanging a virtual photon of excitation. Common examples can be found among noble gas and alkali-metal atoms such as Xe [25] or Na [29]. Two such atoms, initially approaching each other on their molecular ground state, will reverse their trajectories and separate if an optical field resonantly couples the molecular ground state to a repulsive excited state at a well-localized internuclear distance. This effective repulsion between the colliding atoms prevents them from reaching the short-range region where inelastic processes could lead to trap loss. The atoms are then said to be ''shielded'' from reactive or excitation processes, and the corresponding decreased collision rates are said to be ''suppressed.'' Since the interaction involved is repulsive, it follows that the shielding light field has to be tuned to the blue of the atomic transition frequency in order to be resonant with the quasimolecular system. The internuclear distance R_C around which the excitation is localized is called ''the Condon point.'' Thus the atoms never get closer together than about R_C and inelastic collision processes due to interactions at much shorter distances are strongly diminished. Figure 1 shows a sketch of this basic description.

Although the shielding phenomenon has been semiquantitatively explained by two-state Landau-Zener models [23,28], these models are greatly oversimplified and can be misleading. In fact, the two-state Landau-Zener picture predicts that photoassociative ionization in Na [24] and Penning ionization of trapped Xe metastable are suppressed at high laser intensity much more effectively than is observed [12,30]. This failure to achieve complete shielding implies a limitation on the process that must be understood. In this work we go beyond the limits of two-state models by setting up a close-coupled three-dimensional quantum scattering calculation for the collision

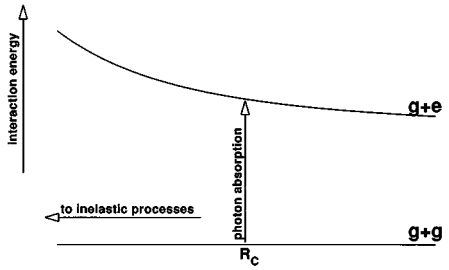

FIG. 1. Sketch of the basic idea of suppression of collision rates of laser-cooled atoms. Two atoms in their ground states $(g+g)$ approach each other and a photon is absorbed at about the Condon point R_C. Then the interaction energy between the atoms becomes repulsive and the quasimolecule dissociates in one ground-state and one excited-state atom $(g+e)$. This process strongly diminishes inelastic collisions occurring at distances shorter than R_C.

$$A(^1S)+A(^1S)+P(\hat{\hat{\boldsymbol{\varepsilon}}}_q,\hbar\omega_L)\rightarrow A(^1S)+A(^1P), \qquad (1)$$

where $A(^1S)$ stands for an atom in its ground state of symmetry ^1S, $A(^1P)$ stands for an atom in its first excited state of symmetry ^1P, and $P(\hat{\hat{\boldsymbol{\varepsilon}}}_q,\hbar\omega_L)$ represents a photon of energy $\hbar\omega_L$ and polarization unit vector $\hat{\hat{\boldsymbol{\varepsilon}}}q$, where $q=0$ for linear polarization and $q=\pm 1$ for circular polarization. This model represents real scattering of group II atoms (Mg, Ca, etc.) and may serve as a qualitative guide for understanding effects in more complex atoms like Xe or Na. Indeed, a recent experiment [12], suggested by the present calculations, confirms our qualitative predictions. This experiment shows that optical suppression of photoassociative ionization of ultracold sodium atoms is dramatically sensitive to the intensity and polarization of the suppressor field. As intensity increases, shielding by circularly polarized light is more efficient than by linearly polarized light, a result that is in qualitative agreement with the predictions we can make by using our three-dimensional model. Choosing Eq. (1) eliminates spin issues, since only singlet states are involved, and allows us to treat field-dressing effects quite straightforwardly. Of course the fine and hyperfine structures are important for real alkali-metal and noble gas systems at ultracold temperatures [29], but are too complex to be incorporated in a theoretical description of strong-field effects in a first attempt. Here we present a rigorous, fully quantum mechanical calculation to investigate physical effects not predictable by simple two-channel models. It is essential to emphasize at this point that we use a standard scattering theory approach to solve exactly a three-dimensional model including light polarization. We treat exactly the effects of the radiation field as power increases and the light is no longer a weak perturbation on the collision. With this rigorous three-dimensional model we investigate the validity of simple two-channel models that have been proposed and show that they are not capable of describing the saturation regime correctly. It is not possible to calculate the saturation behavior if the full fine and hyperfine structures are included in the theory. Although the light field interaction can be exactly introduced together with the fine and hyperfine structures in the weak-field limit [31], we cannot solve this multichannel problem for the strong-field case because the number of coupled equations will become impracticably large. However, in this paper we show that the multichannel character of this simplified three-dimensional model, although excluding internal spin structure, has a dramatic effect on optical shielding of colliding ultracold atoms. Similar effects will certainly be strong also in collisions between real alkali-metal atoms including fine and hyperfine structures, but here we take just the first step towards investigating these effects.

Let $\hbar\omega_0$ be the energy separation associated with the atomic transition $^1S \rightarrow {}^1P$. To further simplify the model, we work at a large enough detuning $\Delta\equiv\omega_L-\omega_0$ that spontaneous decay of the upper state during the shielding interaction can be ignored, as shown by Suominen *et al.*. [28]. In this work we consider the case in which $\Delta=500$ MHz, corresponding to approximately 50 natural linewidths of the assumed atomic transition $^1S \rightarrow {}^1P$.

Room temperature collisions in a strong field are known to saturate differently from a two-state Landau-Zener model due to multiple photon exchanges during the scattering process [32]. We show that the same is true at ultracold collision energies and that the shielding phenomenon depends strongly on the photon polarization. In the following, we will consider an energy $E/k_B=240$ μK, where 240 μK is equal to the Doppler cooling limit temperature T_D for sodium [10].

In this work we consider only one energy and detuning for three reasons. First, our aim is to show how, for a typical collision energy and detuning, the three-dimensional physical picture is different from the one-dimensional picture. Second, the length of the calculations makes surveying a wide range of conditions difficult. Third, the experiments [12,24] have only been reported at a detuning close to the one used in these calculations. We have done some calculations for different energies and from our results it is apparent that a thermal average would not be qualitatively different from the results shown here. In a future paper we plan to present very low temperature results in the regime appropriate for Bose-Einstein condensation.

This paper is organized as follows. In Sec. II we describe the formulation of the standard close-coupling scattering theory to treat Eq. (1), taking into account the high-intensity-field issues involved. We begin by defining the asymptotic basis set of states, which specify the entrance and exit channels. Then we establish the correlation between these asymptotic states and the molecular basis set. Next we discuss the total Hamiltonian and present a brief outline of standard close-coupling theory to define the equations to be solved. We introduce the S matrix by imposing scattering boundary conditions to the solutions of the coupled equations and write down the cross sections for the processes of penetration to the inner region, production of excited states, and elastic scattering in terms of the T-matrix elements. Since in this paper we are considering bosons, we give a brief analysis of indistinguishability and derive its consequences relevant to the present calculations. We obtain the probability of penetration into the inner region by introducing an artificial channel that is coupled only to the ground-state inner wall. Finally, we present the Born-Oppenheimer potential curves and describe the matrix representing the Hamiltonian used in the code to solve this problem.

In Sec. III we describe the numerical outcome of this close-coupling theory. We present the rate coefficients [19] relevant to this work and define the shielding measure as the probability of penetration into the inner region, considering the contribution of different partial waves. Next we present the two-state Landau-Zener theory and show the striking dependence of optical shielding on light polarization. We also predict that the shielding measure has an anisotropic character due to the fact that the higher l-wave contributions can be appreciable. Then we show the results of excited-state production and compare them with the Landau-Zener model. Finally, we present the results for elastic-scattering, showing the increase in orders of magnitude of the rate coefficient for a few W/cm^2 of increase in intensity. In Sec. IV we summarize the main results of this work, outlining their significance for future research.

II. DESCRIPTION OF THE MODEL

A collision in the presence of a blue-detuned light field near atomic resonance can have three consequences: the shielding of an inelastic process that occurs when the atoms penetrate closer than R_C, production of hot excited atoms, and modified ground-state elastic scattering. Our goal in this section is to set up an exact three-dimensional quantum scattering calculation for the effect on the rates of all three processes. We have to describe the collision in a strong radiation field of polarization $\hat{\vec{\varepsilon}}_q$ where the arbitrary collision axis makes an angle $\theta_{\hat{\varepsilon}_q}$ with $\hat{\vec{\varepsilon}}_q$. We first must set up the basis that describes the asymptotically separated field-dressed atoms quantized in a space-fixed frame defined by $\hat{\vec{\varepsilon}}_q$. Then we must describe the rotating symmetric top basis set for the quasimolecule formed when the two atoms are close enough together to interact. Knowing the transformation between these separated-atom and quasimolecular basis sets lets us set up the coupled equations which describe the collision dynamics in a radiation field. Since the field breaks the rotational symmetry of free space by imposing a preferred direction, the quasimolecular total angular momentum is not a good quantum number, and we generate an infinite set of coupled equations. In practice, these can be truncated after a few angular momenta, and solutions can be obtained. Imposing standard boundary conditions lets us extract the S-matrix elements that describe ground- and excited-state collisions of the dressed atoms as functions of the laser intensity I and $\theta_{\hat{\varepsilon}_q}$. We will explain how this is done in the following subsections with further details given in the Appendices. We follow the procedure for weak-field collisions of type (1) set up by Julienne and Mies [33,34] generalized to the case of strong fields. We also point out that, since we are emphasizing the effects of strong electromagnetic interactions on the colliding system, we have neglected the radial and angular nonadiabatic Born-Oppenheimer couplings (see Appendix C). We are justified in disregarding these contributions because, according to the Born-Oppenheimer expansion of the Hamiltonian in terms of the dimensionless parameter $(m/M)^{1/4}$, where m is the electron mass and M is the nuclear mass, the nonadiabatic couplings are of fifth and higher order in this parameter, while the ones we have considered are of the fourth and lower order [35].

A. Asymptotic basis set

To calculate collision rates for Eq. (1), let us first write down the relevant basis of states at a very large separation of the two approaching atoms. In such a situation, we can neglect any interaction between the two atoms and separate their electronic motions from the relative rotational motion of the nuclei. Let us choose a space-fixed right-handed frame of coordinates. Let $\vec{R}$ be the vector from one of the nuclei to the other. Therefore, the relative rotational motion of the two atoms is described by the set of all spherical harmonic functions $Y_l^{m_l}(\theta,\varphi)$ $(l=0,1,2,\ldots;\ m_l=-l,-l+1,\ldots,l-1,l)$, where θ and φ are the polar angles of $\vec{R}$ defined by the relations

$$\hat{\vec{x}}\cdot\vec{R}=|\vec{R}|\sin\theta\cos\varphi, \tag{2a}$$

$$\hat{\vec{y}}\cdot\vec{R}=|\vec{R}|\sin\theta\sin\varphi, \tag{2b}$$

$$\hat{\vec{z}}\cdot\vec{R}=|\vec{R}|\cos\theta, \tag{2c}$$

where $\hat{\vec{x}}$, $\hat{\vec{y}}$, and $\hat{\vec{z}}$ are the unit vectors parallel to the x, y, and z axes, respectively. Later we will assume that the two nuclei are identical bosons and we will show that, as a consequence, only even values of l are involved in the scattering process of Eq. (1). For the moment, however, we suppose the two nuclei are isotopes that can be distinguished one from the other. This restriction will be withdrawn when we consider the calculation of the scattering cross sections. To formalize the issue of the relative rotational motion, let $\vec{l}\equiv -i\hbar\vec{R}\times\vec{\nabla}_{\vec{R}}$. Therefore

$$\vec{l}^{\,2}Y_l^{m_l}(\theta,\varphi)=l(l+1)\hbar^2Y_l^{m_l}(\theta,\varphi), \tag{3a}$$

$$\hat{\vec{z}}\cdot\vec{l}\,Y_l^{m_l}(\theta,\varphi)=m_l\hbar Y_l^{m_l}(\theta,\varphi). \tag{3b}$$

Asymptotically, the motion of the electrons of both atoms can be expanded in terms of basis states of definite total electronic angular momentum. Let us add together the total electronic angular momenta of both colliding atoms and denote the resulting quantum number by j. The two relevant situations, according to Eq. (1), correspond, first, to two atoms in their ^1S ground states, and, second, to one atom in its ^1S ground state and the other in its ^1P first excited state. Thus the first situation is characterized by $j=0$ and the second by $j=1$. Hence we denote the relevant electronic basis states by $|j,m_j\rangle$ ($m_j=0$ for $j=0$; and $m_j=0,\pm1$ for $j=1$), where m_j is the quantum number associated with the projection of the total electronic angular momentum operator $\vec{j}$ along $\hat{\vec{z}}$. Summarizing,

$$\vec{j}^{\,2}|j,m_j\rangle=j(j+1)\hbar^2|j,m_j\rangle, \tag{4a}$$

$$\hat{\vec{z}}\cdot\vec{j}\,|j,m_j\rangle=m_j\hbar|j,m_j\rangle. \tag{4b}$$

In the absence of laser light, the asymptotic basis set describing the two-atom system, including nuclear motion, is given by all the states $|j,m_j\rangle Y_l^{m_l}(\theta,\varphi)$.

B. Correlation between asymptotic and molecular basis sets

To correlate the states of this separated-atom system with the states of the quasimolecular system, let us express $|j,m_j\rangle$ in terms of its body-fixed counterparts $|j,\Lambda\rangle$, where Λ is defined by the eigenvalue equation

$$\frac{\vec{R}\cdot\vec{j}}{|\vec{R}|}|j,\Lambda\rangle=\Lambda\hbar|j,\Lambda\rangle. \tag{5}$$

Thus from Eqs. (4) and the isotropy of space, it follows that $\Lambda=0,\pm1$. As $R\equiv|\vec{R}|\to\infty$, the states $|j,\Lambda\rangle$ do not depend on R, for, as is expected, one atom does not interact with the other asymptotically. As R decreases, the interaction between the atoms increases and the motion of the electrons couples with the interatomic axis in such a way that j is no

longer a good quantum number [36]. However, because of the cylindrical symmetry of the quasimolecule, Λ is still a good approximate quantum number even for very small R. The total angular momentum $\vec{J}=\vec{j}+\vec{l}$ (neglecting nuclear spins) is a good quantum number in the absence of light. Thus at short enough R, Hund's coupling case (a) is applicable [36] and, neglecting retardation effects, the molecular wave functions relevant to the process of Eq. (1) are given by [37]

$$|R,j=0,\Lambda=0,J,M_J\rangle \equiv \Theta^J_{M_J,\Lambda=0}(\theta,\varphi)|0,{}^1\Sigma_g^+(R),\Lambda=0\rangle, \tag{6a}$$

$$|R,j=1,\Lambda=0,J,M_J\rangle \equiv \Theta^J_{M_J,\Lambda=0}(\theta,\varphi)|1,{}^1\Sigma_u^+(R),\Lambda=0\rangle, \tag{6b}$$

$$|R,j=1,\Lambda=\pm 1,J,M_J\rangle \equiv \Theta^J_{M_J,\Lambda=\pm 1}(\theta,\varphi)|1,{}^1\Pi_u(R),\Lambda=\pm 1\rangle, \tag{6c}$$

where $\Theta^J_{M_J,\Lambda}(\theta,\varphi)$ are the symmetric top eigenfunctions introduced by Eq. (A5) of Appendix A; $|0,{}^1\Sigma_g^+(R),\Lambda=0\rangle$ is the electronic ground state of the molecule formed by the two colliding atoms, it has the symmetry ${}^1\Sigma_g^+$ and correlates with the electronic state of the separated atoms in their ground states; $|1,{}^1\Sigma_u^+(R),\Lambda=0\rangle$ and $|1,{}^1\Pi_u(R),\Lambda=\pm 1\rangle$ are the molecule electronic states, of symmetries ${}^1\Sigma_u^+$ and ${}^1\Pi_u$, respectively, that correlate with the electronic states of the separated atoms when one of them is in its ground state and the other is in its first excited state. For simplicity, we will assume that ${}^1S$ has even parity and ${}^1P$ has odd parity, thus the molecule excited-state symmetry ${}^1\Sigma_u^+$ is present and not ${}^1\Sigma_u^-$ [36].

C. The Hamiltonian

In this model, the Hamiltonian H consists of three parts:

$$H=H_0+H_F+H_I, \tag{7}$$

where H_0 is the quasimolecule Hamiltonian, H_F is the laser-field Hamiltonian, and H_I is the interaction Hamiltonian between the quasimolecule and the electric field. H_0 is given by

$$H_0=-\frac{\hbar^2}{2\mu}\vec{\nabla}_R^2+V(R), \tag{8}$$

where μ is the reduced mass of the two colliding atoms, $-(\hbar^2/2\mu)\vec{\nabla}_R^2$ is the kinetic energy operator of the two atoms about their center of mass, and $V(R)$ is the interaction energy of the two atoms that depends on the internuclear separation R and the electronic variables. Let us denote the eigenvalue of the operator $V(R)$ associated with the eigenvector $|R,j,\Lambda,J,M_J\rangle$ by $V^j_{|\Lambda|}(R)$:

$$V(R)|R,j,\Lambda,J,M_J\rangle=V^j_{|\Lambda|}(R)|R,j,\Lambda,J,M_J\rangle, \tag{9}$$

where we suppose no Λ doubling and thus the states with $\Lambda=\pm 1$ are degenerate. The functions $V^j_{|\Lambda|}(R)$ are the usual Born-Oppenheimer potentials. Because the zero of energy is arbitrary, let $V^0_0(\infty)=0$ and $V^1_{|\Lambda|=0,1}(\infty)=\hbar\omega_0$. Since we are considering a situation in which there is only one laser mode populated by n_L photons and spontaneous emission is not important, the Hamiltonian for the laser field is written

$$H_F=\hbar\omega_L(a_q^\dagger a_q-n_L), \tag{10}$$

where $a_q^\dagger$ is the operator that creates a photon of frequency ω_L and polarization unit vector $\hat{\vec{\varepsilon}}_q$, a_q is the corresponding annihilation operator, and we have chosen the zero of field energy as the eigenvalue of the state with n_L photons. In the electric dipole approximation, for $R\ll c/\omega_L$ [38], the interaction Hamiltonian H_I is written

$$H_I=-i\left(\frac{2\pi\hbar\omega_L}{V_Q}\right)^{1/2}\vec{\mu}_M\cdot(\hat{\vec{\varepsilon}}_q a_q-\hat{\vec{\varepsilon}}_q^* a_q^\dagger), \tag{11}$$

where V_Q is the quantization volume and $\vec{\mu}_M$ is the molecular electric dipole operator.

It will become clear when we apply the scattering boundary conditions that it is necessary to use a basis in which H is asymptotically diagonal. Thus it is natural to treat the two-atom system and the laser in the dressed picture. Let $|n_L\rangle$ denote the laser state in which there are n_L photons of frequency ω_L and polarization unit vector $\hat{\vec{\varepsilon}}_q$. The electromagnetic interaction with the two-atom system will couple the state $|j=0,m_j=0\rangle Y_l^{m_l}(\theta,\varphi)|n_L\rangle$ with the state $|j=1,m_j=q\rangle Y_l^{m_l}(\theta,\varphi)|n_L-1\rangle$ and the corresponding matrix element is the Rabi frequency Ω,

$$\hbar\Omega=-i\left(\frac{2\pi}{c}I\right)^{1/2}\langle j=1,m_j=q|\hat{\vec{\varepsilon}}_q\cdot\vec{\mu}_M|j=0,m_j=0\rangle, \tag{12}$$

which we can choose as a real quantity due to the arbitrariness of the global phase factors of the quantum states. Here I is the intensity of the laser field:

$$I\equiv\frac{\hbar c\omega_L}{V_Q}n_L. \tag{13}$$

It is worth remarking that some authors define the Rabi frequency as one-half the matrix element in Eq. (12) [39]. For fixed l and m_l, the total Hamiltonian H is asymptotically diagonal if written in the dressed-state basis spanned by

$$|D_\beta(R),l,m_l\rangle\equiv\sum_{\gamma=1}^{4}M_{\beta,\gamma}|U_\gamma(R),l,m_l\rangle \tag{14}$$

for $\beta=1,2,3,4$, where

$$|U_1(R),l,m_l\rangle\equiv|R,j=0,m_j(1),l,m_l\rangle|n_L\rangle, \tag{15a}$$

$$|U_\gamma(R),l,m_l\rangle\equiv|R,j=1,m_j(\gamma),l,m_l\rangle|n_L-1\rangle, \tag{15b}$$

for $\gamma=2,3,4$, with $m_j(1)\equiv 0$, $m_j(2)\equiv q(q-1)/2-1$, $m_j(3)\equiv 1-q(q+1)/2$, and $m_j(4)\equiv q$;

$$|R,j,m_j,l,m_l\rangle \equiv \sum_{J,M_J,\Lambda} \sqrt{\frac{2l+1}{2J+1}}\langle j,l,m_j,m_l|J,M_J\rangle \times\langle j,l,\Lambda,0|J,\Lambda\rangle|R,j,\Lambda,J,M_J\rangle \quad (16)$$

(see Appendix A); and $M_{\beta,\gamma}$ are the matrix elements of

$$[M]=\begin{bmatrix} A_+ & 0 & 0 & B_+ \\ 0 & 1 & 0 & 0 \\ 0 & 0 & 1 & 0 \\ A_- & 0 & 0 & B_- \end{bmatrix}, \quad (17)$$

where

$$A_\pm \equiv \frac{\pm\hbar\Omega}{\sqrt{E_\pm^2+(\hbar\Omega)^2}}, \quad (18a)$$

$$B_\pm \equiv \frac{\pm E_\pm}{\sqrt{E_\pm^2+(\hbar\Omega)^2}} \quad (18b)$$

and

$$E_\pm = \frac{\hbar(-\Delta\pm\sqrt{\Delta^2+4\Omega^2})}{2}. \quad (18c)$$

The basis states given by Eq. (14) are the states prepared or detected in the asymptotic region. These are the states we need to define the S matrix, since they describe two isolated atoms in a radiation field, separated by a large distance.

In this work we use a conservative Hamiltonian treatment and neglect spontaneous emission. The shielding dynamics is primarily associated with the effect the field has on the quasimolecule in the vicinity of the Condon point. When the detuning is large enough, the excited $1/R^3$ molecular potential induces a strong acceleration to the atoms. Hence the atoms do not spend enough time near the Condon point to spontaneously emit photons. A rigorous treatment of the spontaneous emission requires a full density matrix approach [28,30]. Such density matrix calculations indicate that spontaneous emission can be neglected near the Condon point if $\Delta \gg \gamma$. Based on these results, our choice of $\Delta = 500$ MHz and $\gamma \approx 10$ MHz justifies neglecting spontaneous emission near the Condon point. We also neglect spontaneous emission occurring asymptotically, because the light field intensities we consider are not high enough to populate the undressed excited states appreciably.

D. Close-coupling theory

The standard close-coupling equations are given by [40,41]

$$\langle D_{\beta''}(R),l'',m_l''|(H-E)|\Psi_{\beta',l',m_l'}(E,R)\rangle = 0, \quad (19)$$

where

$$|\Psi_{\beta',l',m_l'}(E,R)\rangle \equiv \sum_{\beta=1}^{4}\sum_{l=0}^{\infty}\sum_{m_l=-l}^{+l} \frac{F^{\beta,l,m_l}_{\beta',l',m_l'}(E,R)}{R} \times|D_\beta(R),l,m_l\rangle, \quad (20)$$

E is the total energy of the colliding pair, and the coefficients $F^{\beta,l,m_l}_{\beta',l',m_l'}(E,R)$ are required to satisfy boundary conditions suitable for scattering processes:

$$F^{\beta',l',m_l'}_{\beta,l,m_l}(E,\infty) = i\left(\frac{\mu}{2\pi\hbar^2 k_\beta}\right)^{1/2}\delta_{\beta,\beta'}\delta_{l,l'}\delta_{m_l,m_l'}e^{-i(k_\beta R-\pi l/2)} - i\left(\frac{\mu}{2\pi\hbar^2 k_{\beta'}}\right)^{1/2} e^{i(k_{\beta'}R-\pi l'/2)}S^{\beta',l',m_l'}_{\beta,l,m_l}(E), \quad (21)$$

where $S^{\beta',l',m_l'}_{\beta,l,m_l}(E)$ is the so-called S matrix for the transition from state $|D_\beta\rangle Y_l^{m_l}(\theta,\varphi)$ to state $|D_{\beta'}\rangle Y_{l'}^{m_l'}(\theta,\varphi)$. There is an excellent discussion by Mies [42] about this point and the reader is also referred to Appendix B for details.

E. Scattering cross sections

Defining the T matrix as

$$T^{\beta',l',m_l'}_{\beta,l,m_l}(E) \equiv \delta_{\beta,\beta'}\delta_{l,l'}\delta_{m_l,m_l'} - S^{\beta',l',m_l'}_{\beta,l,m_l}(E), \quad (22)$$

and using Eqs. (20) and (21) allows us to write the scattering amplitude as

$$f_\beta^{\beta'}(\theta_{\vec{k}_\beta},\varphi_{\vec{k}_\beta},\theta,\varphi) = \frac{2\pi}{k_\beta}\sum_{l=0}^{\infty}\sum_{m_l=-l}^{+l}\sum_{l'=0}^{\infty}\sum_{m_l'=-l'}^{+l'} i^{l-l'-1} \times T^{\beta',l',m_l'}_{\beta,l,m_l}(E)Y_l^{m_l*}(\theta_{\vec{k}_\beta},\varphi_{\vec{k}_\beta})Y_{l'}^{m_l'}(\theta,\varphi), \quad (23)$$

where $\theta_{\vec{k}_\beta}$ and $\varphi_{\vec{k}_\beta}$ specify the incident direction (see Appendix B). We can calculate the differential cross section of scattering from state β to β' by the usual procedure [43] and we find

$$\frac{d\sigma_{\beta\to\beta'}(E,\theta_{\vec{k}_\beta},\varphi_{\vec{k}_\beta},\theta,\varphi)}{\sin\theta d\theta d\varphi} = |f_\beta^{\beta'}(\theta_{\vec{k}_\beta},\varphi_{\vec{k}_\beta},\theta,\varphi)|^2. \quad (24)$$

To calculate the total cross section for a transition $\beta\to\beta'$ we proceed by averaging over the incident direction $(\theta_{\vec{k}_\beta},\varphi_{\vec{k}_\beta})$ and integrating over the final direction (θ,φ):

$$\sigma_{\beta\to\beta'}(E) = \frac{1}{4\pi}\int_0^\pi d\theta_{\vec{k}_\beta}\int_0^{2\pi}d\varphi_{\vec{k}_\beta}\int_0^\pi d\theta\int_0^{2\pi} \times d\varphi|f_\beta^{\beta'}(\theta_{\vec{k}_\beta},\varphi_{\vec{k}_\beta},\theta,\varphi)|^2, \quad (25)$$

and from Eqs. (23)–(25) we get

$$\sigma_{\beta\to\beta'}(E)=\frac{\pi}{k_\beta^2}\sum_{l=0}^{\infty}\sum_{m_l=-l}^{+l}\sum_{l'=0}^{\infty}\sum_{m_l'=-l'}^{+l'}|T_{\beta,l,m_l}^{\beta',l',m_l'}(E)|^2. \tag{26}$$

F. Indistinguishability

So far we have been considering two distinguishable nuclei, but now let us determine the required changes in this formulation for the actual case of identical nuclei. The electronic motion for the two-atom system can be described, asymptotically, by linear combinations of products of atomic wave functions. For the ground state, for example, we can write

$$|j=0,m_j=0\rangle=\mathcal{A}_e|S\rangle|S\rangle, \tag{27}$$

where $\mathcal{A}_e$ is the electronic antisymmetrizer operator, the first ket $|S\rangle$ indicates an atom at the origin in its ^1S ground state, and the second ket $|S\rangle$ indicates an atom at infinity in its ^1S ground state. In the case of identical nuclei of zero spin, no changes are necessary in Eq. (27) because the product $|S\rangle|S\rangle$ is symmetrical under exchange of nuclei. For the excited states, if the two nuclei are not identical, we have

$$|j=1,m_j\rangle=\mathcal{A}_e\frac{|S\rangle|P(m_j)\rangle+|P(m_j)\rangle|S\rangle}{\sqrt{2}}, \tag{28}$$

where the first product, $|S\rangle|P(m_j)\rangle$, indicates one atom in its ^1S ground state at the origin and the other in its ^1P excited state, of space-fixed angular momentum projection m_j, at infinity, and the second product, $|P(m_j)\rangle|S\rangle$, indicates one atom in its ^1P excited state, of space-fixed angular momentum projection m_j, at the origin, and the other in its ^1S ground state at infinity. Equation (28) correlates to the ungerade excited states because we have supposed ^1P has odd parity and ^1S even parity. Furthermore, if we exchange nuclei, Eq. (28) remains unchanged, meaning that it represents exactly the situation for two identical boson nuclei. The consequence of Eqs. (27) and (28) being both invariant under nuclei exchange implies that the states of Eq. (14) are also invariant. Therefore, following the procedure thoroughly discussed by Verhaar and co-workers [19,44], we find that only even values of l contribute to the scattering process, since the incident part of the scattering wave function contributes only even values of l and the total Hamiltonian Eq. (7) can only couple states of the same values of l or differing by two units [33]. Hence, for the case of identical atoms, including identical nuclei, the necessary change in Eqs. (20), (23), and (26) is to sum only over even values of l and l'.

Indistinguishability also implies the exclusion of certain states in the molecular basis set $|R,j,\Lambda,J,M_J\rangle$. Since $J=l$ for the ground $^1\Sigma_g^+$ state, only even J values are possible for the ground molecular state. Only odd J values are possible for the excited $^1\Sigma_u^+$ state, whereas both even and odd J values are permitted for the $^1\Pi_u$ state. Dipole selection rules do not permit odd J values in the $^1\Pi_u$ state to couple optically to the ground state for the special case of $M_J=0$ for linearly polarized light only. An important consequence of this special case is a strong difference between shielding for the cases of linear and circular polarized light, as we show below.

G. The artificial channel probe

To probe the amount of flux entering the inner region of the ground-state potential, we use the method of the artificial state [45]. This method consists of introducing an extra potential curve as if there were another electronic probe state coupled to the real states in the problem. We are allowed to choose the most convenient artificial state for a particular purpose. For the present problem, we choose a potential curve that is coupled locally to the classical inner turning point of the ground-state potential $V_0^0(R)$ at very low kinetic energies ($\approx 240\ \mu$K). The changes in the present formalism amount to introducing one more state of index $\beta=5$ and replacing Eq. (17) with

$$[M]=\begin{bmatrix} A_+ & 0 & 0 & B_+ & 0\\ 0 & 1 & 0 & 0 & 0\\ 0 & 0 & 1 & 0 & 0\\ A_- & 0 & 0 & B_- & 0\\ 0 & 0 & 0 & 0 & 1 \end{bmatrix}. \tag{29}$$

We define

$$V(R)|U_5(R),l,m_l\rangle\equiv W_A(R)|U_5(R),l,m_l\rangle, \tag{30}$$

where $W_A(R)$ is the totally arbitrary artificial potential curve:

$$W_A(R)=4\varepsilon_A\left[\left(\frac{\sigma_A}{R}\right)^4-\left(\frac{\sigma_A}{R}\right)^3\right]-\hbar\Delta_A, \tag{31}$$

where we take $\varepsilon_A/hc=1.8\times10^4\ \text{cm}^{-1}$, $\sigma_A=4.1a_0$, and $\Delta_A/2\pi=500$ MHz. Also, we need the coupling matrix element

$$\langle U_\beta(R),l,m_l|V(R)|U_5(R),l',m_l'\rangle=\delta_{\beta,1}\delta_{l,l'}\delta_{m_l,m_l'}D_A(R), \tag{32}$$

where $D_A(R)$ is a function of R localized about the classical inner turning point of $V_0^0(R)$:

$$D_A(R)=hce^{-(R-\sigma_A)^2}, \tag{33}$$

where $D_A(R)/hc$ has a value of 1 cm^{-1} at $R=\sigma_A$ and decreases to e^{-1} cm^{-1} at $R=\sigma_A\pm1a_0$. The artificial state is not coupled to any of the other potential curves except at about the classical inner turning point of $W_0^0(R)$.

H. Potential curves

Let us consider the states $|R,j=0,\Lambda,J,M_J\rangle|n_L\rangle$ and $|R,j=1,\Lambda,J,M_J\rangle|n_L-1\rangle$. These states are eigenstates of the operator

$$W(R)\equiv V(R)+H_F, \tag{34}$$

with eigenvalues

$$W_{|\Lambda|}^j(R)\equiv V_{|\Lambda|}^j(R)-j\hbar\omega_L. \tag{35}$$

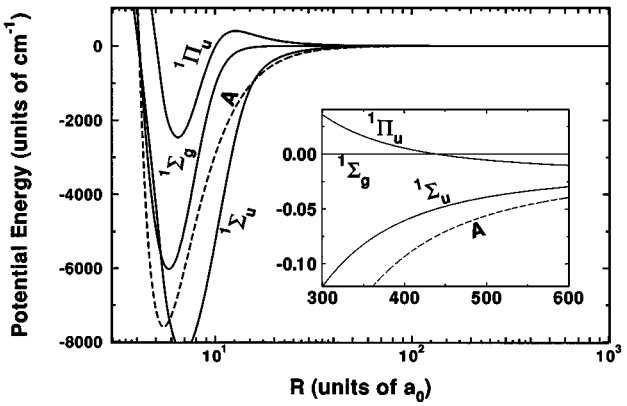

FIG. 2. Potential curves we employ in this work: except for the artificial-channel potential curve labeled ''*A*,'' the others are for Na_2. The curve labeled ''$^1\Sigma_g$'' is identified with $W_0^0(R)$, the one labeled ''$^1\Sigma_u$'' is identified with $W_0^1(R)$, the one labeled ''$^1\Pi_u$'' with $W_1^1(R)$, and ''*A*'' with $W_A(R)$. The inset shows the region of crossing. $R_C \approx 439.24a_0$ is the Condon point for the detuning of 500 MHz.

Figure 2 shows the potential curves $W^j_{|\Lambda|}(R)$ we use in this work. The curve labeled $^1\Sigma_g$ is identified with the ground-state potential curve $W_0^0(R)$. Its short-range part, from $3.8a_0$ to $30a_0$, is the same as used by Thorsheim, Weiner, and Julienne in their paper on laser-induced photoassociation of ultracold sodium atoms [46] for the sodium diatomic molecule Na_2. We point out that these are model calculations, not for real Na-Na collisions, and thus the choice of actual potentials is not crucial. For $R \geqslant 30a_0$, we assume the following extrapolation:

$$W_0^0(R) = -Ae^{-BR} - \frac{C_6}{R^6} - \frac{C_8}{R^8} - \frac{C_{10}}{R^{10}}, \tag{36}$$

where, in atomic units, we take $A = 0.344\,91$, $B = 0.648\,771$, $C_6 = 1\,698$, $C_8 = 102\,810$, $C_{10} = 6\,939\,128$ [47]. The curves labeled $^1\Sigma_u$ and $^1\Pi_u$ correspond, respectively, to the excited-state potential curves $W_0^1(R)$ and $W_1^1(R)$. The short-range portions from $5a_0$ to $52a_0$ of $V_0^1(R)$ and $V_1^1(R)$, which are needed to define $W_0^1(R)$ and $W_1^1(R)$, are cubic spline fits to the data obtained by Magnier *et al.* [48] for the sodium diatomic molecule Na_2. For $R \geqslant 52a_0$, we assume the dipole-dipole resonant interaction, neglecting retardation effects [49]:

$$W_{0,1}^1(R) = -\frac{C_3^{0,1}}{R^3} - \hbar\Delta, \tag{37}$$

where, in atomic units, we take $C_3^1 = -6.439\,846\,4$ for the repulsive curve, and $C_3^0 = 12.823\,449\,6$ for the attractive. All these numbers are chosen so that the extrapolations join smoothly to the potential data. For internuclear separations shorter than $3.8a_0$ or $5a_0$, we extrapolate the curves by straight lines. The form of the potentials for very short range is immaterial due to the fact that the kinetic energies we are considering are much lower than the values of the potential curves at these inner points. Thus there is no appreciable penetration of the wave functions to the linear extrapolation region.

I. Matrix representation of the Hamiltonian

To set up the numerical calculation, we begin by writing the total Hamiltonian H, Eq. (7), in a matrix representation. Let us order the states $|D_\beta(R),l,m_l\rangle$ ($\beta = 1,2,3,4,5$), Eq. (14), in increasing order of l. Therefore, for any pair (m_l,m_l') of integers, let us write the matrix for H as consisting of 5×5 blocks:

$$[H]^{m_l,m_l'} = \begin{bmatrix} \ddots & & \\ & [(l,l)]^{m_l,m_l'}_{5\times 5} & [(l,l+2)]^{m_l,m_l'}_{5\times 5} \\ & [(l+2,l)]^{m_l,m_l'}_{5\times 5} & [(l+2,l+2)]^{m_l,m_l'}_{5\times 5} \\ & & \ddots \end{bmatrix}, \tag{38}$$

where $[(l,l')]^{m_l,m_l'}_{5\times 5}$ is a 5×5 block whose elements are indexed by (β,β') ($\beta,\beta' = 1,2,3,4,5$) and given by

$$([(l,l')]^{m_l,m_l'}_{5\times 5})_{\beta,\beta'} \equiv \langle D_\beta(R),l,m_l|H|D_{\beta'}(R),l',m_l'\rangle, \tag{39}$$

where we define the elements $([(l,l')]^{m_l,m_l'}_{5\times 5})_{\beta,\beta'}$ for which $|m_l| > l$ or $|m_l'| > l'$ as identically zero, so that Eq. (38) is well defined for all pairs (m_l,m_l') of integers. From Eqs. (14) and (29), and the generalization to include $\beta = 5$ in the formalism, we have

$$([(l,l')]^{m_l,m_l'}_{5\times 5})_{\beta,\beta'} = \sum_{\gamma=1}^{5}\sum_{\gamma'=1}^{5} M_{\beta,\gamma}M_{\beta',\gamma'} \times \langle U_\gamma(R),l,m_l|H|U_{\gamma'}(R),l',m_l'\rangle. \tag{40}$$

Appendix C outlines the explicit calculation of the Hamiltonian matrix elements.

The close-coupling equations in matrix form are solved by the numerical procedure of Gordon [50,51]. The S-matrix elements are obtained from the close-coupling solutions by imposing the scattering boundary conditions of Eq. (21). In the next section we present the results obtained by following the prescription described above.

III. RESULTS OF THE NUMERICAL CALCULATIONS

A. Rate coefficients

We define the event rate coefficient for a transition $\beta \to \beta'$ in accordance with Eq. (17) of Ref. [19], namely,

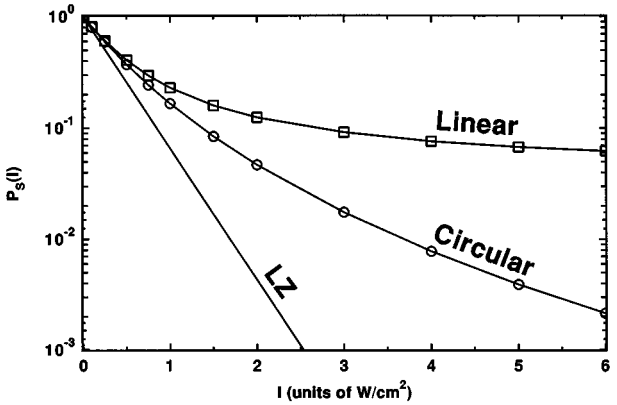

FIG. 3. Numerical results for the shielding measure, $P_S(I)$, as a function of intensity I for linear and circular polarizations. A two-state Landau-Zener model calculation for the s-wave R branch, labeled ''LZ,'' is also shown.

$$K_{\beta\to\beta'}\equiv\left\langle v_{\rm rel}\frac{\pi}{k_\beta^2}\sum_{l=0}^{\infty}\sum_{m_l=-l}^{+l}\sum_{l'=0}^{\infty}\sum_{m_l'=-l'}^{+l'}\left|T_{\beta,l,m_l}^{\beta',l',m_l'}(E)\right|^2\right\rangle_T, \tag{41}$$

where the summations are over even values of l and l' only, $v_{\rm rel}$ is the relative speed at which the atoms approach each other, and $\langle F\rangle_T$ indicates the result of averaging any quantity F over the distribution of relative speeds $v_{\rm rel}$. The rate coefficients of Eq. (41) are used in the rate equation that describes all possible transitions among the states β [19]. For the purposes of this work we take only one value of $v_{\rm rel}$, corresponding to

$$\frac{\mu v_{\rm rel}^2}{2k_B}=240\mu K, \tag{42}$$

where k_B is Boltzmann's constant. We have chosen 240 μK for the collision energy because we are using sodium potentials and the typical temperatures one usually finds in traps of laser-cooled sodium atoms is of the order of the Doppler cooling limit temperature $T_D=240$ μK. Therefore instead of Eq. (41) we use

$$K_{\beta\to\beta'}=v_{\rm rel}\frac{\pi}{k_\beta^2}\sum_{l=0}^{\infty}\sum_{m_l=-l}^{+l}\sum_{l'=0}^{\infty}\sum_{m_l'=-l'}^{+l'}|T_{\beta,l,m_l}^{\beta',l',m_l'}(E)|^2. \tag{43}$$

B. Shielding measure

We generalize the definition of ''shielding measure'' of Suominen *et al.* [28] by

$$P_S(I)\equiv\frac{K_{1\to5}(I)}{K_{1\to5}(I=0)}, \tag{44}$$

where I is the intensity of the laser beam as defined by Eq. (13). $P_S(I)$ is independent of the nature of the artificial state and its coupling to the ground state, because the Condon point and the artificial state coupling with the ground state are very far apart and localized. Figure 3 shows $P_S(I)$ calculated numerically for linear and circular polarizations, as well as the results of a two-state Landau-Zener model which we will describe shortly. The numerical results are obtained by solving the coupled equations for a truncated range of values of l, which is chosen so that the cross sections are converged up to four or five significant figures for the $1\to2,3,4,5$ transitions, and up to two significant figures for the $1\to1$ transitions. For the elastic-scattering, many partial waves are necessary at high intensities, reducing the efficiency of the calculation. Both computing time and the restriction that there is negligible population in the atomic excited state asymptotically cause us to restrict the calculations to a maximum intensity of 6 W/cm^2.

C. Partial waves contributing to shielding measure

Before we proceed, let us notice some details of the formalism and establish a partial-wave nomenclature that will be useful in the discussion that follows. From Eqs. (A2), (A5), (6), and (16), it follows that

$$|U_1(R),l,m_l\rangle=Y_l^{m_l}(\theta,\varphi)|0,{}^1\Sigma_g^+(R),\Lambda=0\rangle|n_L\rangle. \tag{45}$$

Therefore the state $|U_1(R),l,m_l\rangle$ is an eigenstate of $\vec{l}^{\,2}$ for all R. At low intensities, $|D_\beta(R),l,m_l\rangle\to|U_\beta(R),l,m_l\rangle$ ($\beta=1,2,3,4,5$). We call a state such as $|D_\beta(R),l,m_l\rangle$ or $|U_\beta(R),l,m_l\rangle$ an ''l wave'' because, at $R\to\infty$, both are proportional to $Y_l^{m_l}(\theta,\varphi)$. If $l=0$, we call the state an ''s wave,'' if $l=2$, we call it a ''d wave,'' and if $l=4$, we call it a ''g wave.''

For $I=0$ and $E/k_B=240$ μK, only the s wave can penetrate the inner region of the ground-state potential because of the centrifugal barriers for the other partial waves. For example, the d-wave barrier in the ground state is about 20 times higher than $E/k_B=240$ μK. As I increases, partial waves other than the s wave can contribute to $\sigma_{1\to5}$ due to absorption and stimulated emission of more than one photon during the collision. Let us suppose the two colliding atoms approach each other in the long-range region of the ground-state potential as an l wave. At about R_C, the quasimolecule interacts with the electromagnetic field, which can stimulate the absorption and emission of several photons. Therefore, to penetrate the inner region of the ground-state potential and make a transition to the artificial state, the quasimolecule must end up in the ground state as an s wave after interacting with the light at about R_C. An s wave in the ground state has $m_l=0$. A transition from a ground-state l wave to a ground-state s wave conserves m_l because a photon cannot ''torque'' the nuclear angular momentum. Hence an arbitrary l wave in the ground state can contribute to $\sigma_{1\to5}$ only if it has $m_l=0$. This consequence is important in selecting the relevant diagonalized potential curves for all the states in a range of values of l: from all the possible potential curves, only the ones with $m_l=0$ in the ground state are relevant to study the shielding measure.

D. Two-state Landau-Zener theory

Now let us consider the regime of very low intensity and present the two-state Landau-Zener model. Since in this regime we expect only the s wave in the ground state to con-

tribute to $P_S(I)$, only the 5×5 block with $l=0$ in Eq. (38) is necessary to describe the physical situation. In this low-intensity limit, it follows from Eqs. (15) and (C11) that the s-wave state $Y_{l=0}^{m_l=0}(\theta,\varphi)|0,{}^1\Sigma_g^+(R),\Lambda=0\rangle|n_L\rangle$ is coupled, electromagnetically, only to the state $|U_4(R),l'=0,m_l'=0\rangle$. Therefore from Eq. (16) we obtain

$$
\begin{aligned}
&|U_4(R),l'=0,m_l'=0\rangle \\
&\quad=\frac{1}{\sqrt{3}}|R,j=1,\Lambda=0,J=1,M_J=q\rangle|n_L-1\rangle \\
&\qquad+\frac{1}{\sqrt{3}}|R,j=1,\Lambda=1,J=1,M_J=q\rangle|n_L-1\rangle \\
&\qquad+\frac{1}{\sqrt{3}}|R,j=1,\Lambda=-1,J=1,M_J=q\rangle|n_L-1\rangle. \qquad (46)
\end{aligned}
$$

Thus the relevant body-fixed excited states are $|R,j=1,\Lambda,J=1,M_J=q\rangle|n_L-1\rangle$ for $\Lambda=-1,0,1$, and the corresponding eigenvalues of the potential operator $W(R)$ are $W^1_{|\Lambda|=0,1}(R)$. From Fig. 2 we see that only $W^1_{|\Lambda|=1}(R)$ crosses $W^0_0(R)$ at R_C. Therefore we can neglect the excited state with $\Lambda=0$ because it is nonresonant and we are left with the two degenerate excited states with $\Lambda=-1,1$. Let us consider the linear combinations

$$
\begin{aligned}
|\pm\rangle\equiv&\frac{1}{\sqrt{2}}|R,j=1,\Lambda=1,J=1,M_J=q\rangle|n_L-1\rangle \\
&\pm\frac{1}{\sqrt{2}}|R,j=1,\Lambda=-1,J=1,M_J=q\rangle|n_L-1\rangle. \qquad (47)
\end{aligned}
$$

The state $|+\rangle$ has odd parity and the state $|-\rangle$ has even parity, as can be checked by inverting Eq. (16) and using Eqs. (27) and (28). Since the electric dipole operator is a vector operator, it follows that only $|+\rangle$ is coupled electromagnetically to the s-wave state. Because the s wave has $J=0$ and $|+\rangle$ has $J'=1$, this transition is an R-branch transition. From Eqs. (12), (C4), (C5), (C9), and (C12), and the Wigner-Eckart theorem [52], we obtain the following Rabi frequency for the two-level system involving only state $|+\rangle$ and the s wave:

$$\Omega_{\rm LZ}=\frac{2}{\sqrt{3}}\Omega^A. \qquad (48)$$

We have thus reduced the problem to a two-state model in this low-intensity regime. The dynamics in the region of the crossing can be described by a Landau-Zener model as described by Suominen *et al.* [28]. In this theory, the probability for the system to remain in the s-wave state after passing through the crossing at R_C is given by

$$P_S^{\rm LZ}=\exp\left(-\frac{2\pi\hbar\Omega_{\rm LZ}^2}{v\,\alpha_{\rm LZ}(R_C)}\right), \qquad (49)$$

where

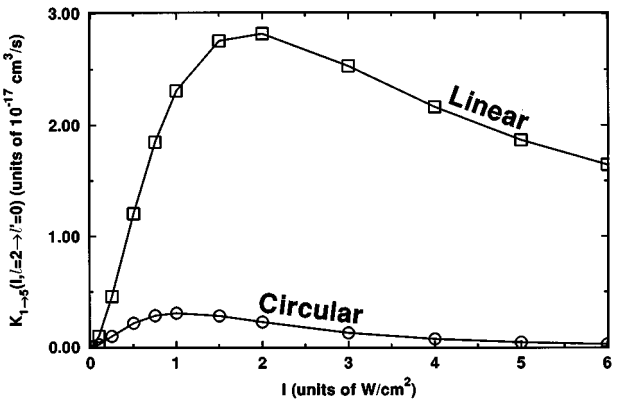

FIG. 4. Contribution of the d wave to the rate coefficient for linear and circular polarizations.

$$\alpha_{\rm LZ}(R)\equiv\left|\frac{d}{dR}[W_1^1(R)-W_0^0(R)]\right|, \qquad (50)$$

and v is the relative speed of the atoms at the crossing position R_C. Equation (49) is the shielding measure according to the Landau-Zener theory. For our choice of parameters and potential curves, $P_S^{\rm LZ}$ of Eq. (49) can be expressed as a function of laser intensity I in W/cm^2 as

$$P_S^{\rm LZ}(I)=\exp[-2.7239I(W/{\rm cm}^2)]. \qquad (51)$$

If we define the saturation intensity I_S of the Landau-Zener shielding measure as the intensity at which $P_S^{\rm LZ}(I=I_S)=1/e$, we obtain, from Eq. (51), $I_S\approx367$ mW/cm^2. Figure 3 shows that the Landau-Zener model of shielding measure approaches zero much faster than the linear or circular three-dimensional calculations. The three curves start very close to one another at low intensities, and then diverge appreciably. This low-intensity behavior is expected, since in this case all three curves involve the entrance s wave only, and therefore the three-dimensional results are equivalent to the two-state R-branch Landau-Zener model. Only when the d wave begins to participate as intensity increases do the curves diverge.

E. Light polarization dependence of optical shielding

Figure 4 shows the contribution of the d wave to the shielding measure, as calculated by the three-dimensional approach. The quantity $K_{1\to5}(I,l=2\to l'=0)$ of Fig. 4 is the contribution to the rate coefficient, Eq. (43), arising from the terms with $l=2$ and $l'=0$. In general, we define

$$K_{\beta\to\beta'}(I,l\to l')\equiv\frac{\pi v_{\rm rel}}{k_\beta^2}\sum_{m_l=-l}^{+l}\sum_{m_l'=-l'}^{+l'}|T^{\beta',l',m_l'}_{\beta,l,m_l}(E)|^2. \qquad (52)$$

The difference in behavior for linear and circular polarizations is evident in Fig. 4, which shows that the d-wave contribution in the linear case is over one order of magnitude larger than in the circular case. Before analyzing the reasons why there is such a difference, let us examine the g-wave contribution to the rate coefficient for both polarization cases. Figure 5 shows the quantity $K_{1\to5}(I,l=4\to l'=0)$ for

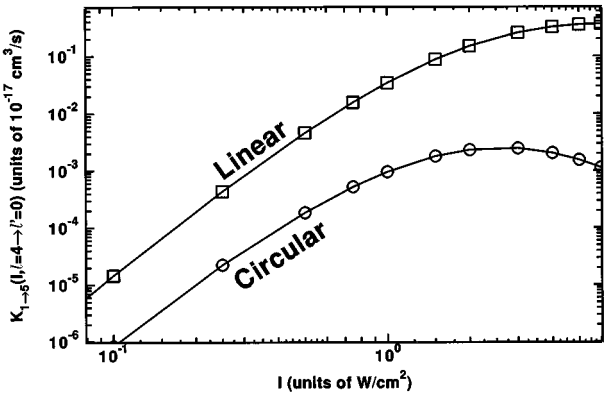

FIG. 5. Contribution of the g wave to the rate coefficient for linear and circular polarizations.

linear and circular polarizations. The contribution of the g wave in the linear case is about two orders of magnitude larger than in the circular case. Furthermore, for linear polarization, the g-wave contribution is about one order of magnitude smaller than the d-wave contribution; and for circular polarization, the g-wave contribution is about two orders of magnitude smaller than the d-wave contribution.

It is apparent from Figs. 4 and 5 that the key to understanding the polarization dependence of the shielding measure is in the different order of magnitudes of the corresponding d-wave contributions. To appreciate the fact that we do not need to consider contributions of partial waves much higher than the d wave, Fig. 6 shows the quantity

$$K_{1\to5}^{\text{partial}}(I)\equiv K_{1\to5}(I,l=0\to l'=0)+K_{1\to5}(I,l=2\to l'=0)+K_{1\to5}(I,l=4\to l'=0), \tag{53}$$

together with the total rate coefficient, Eq. (43), for linear and circular polarizations.

To interpret these results, it is useful to concentrate on the Hamiltonian matrix, Eq. (38), for the case in which we include the blocks for $l=0$ and $l=2$ for $m_l=0$ in the ground state. Equation (38) minus the matrix for the radial term, $-[(\hbar^2/2\mu)(1/R)(\partial^2/\partial R^2)]R$, can be diagonalized and the resulting adiabatic potential curves near the Condon point

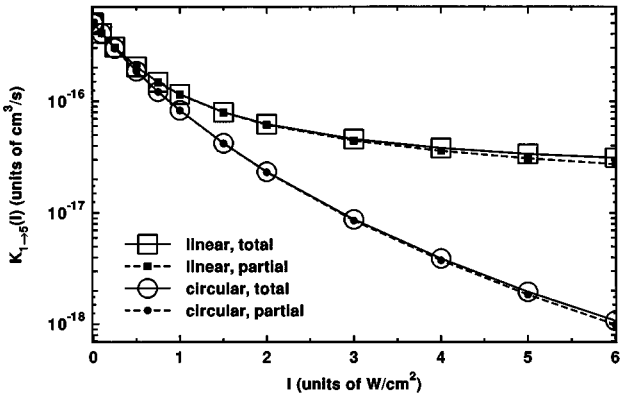

FIG. 6. Comparison between the partial and total rate coefficients for linear and circular polarizations. The items in the legend refer, first, to the polarization case, and, second, to the total or partial rate coefficients.

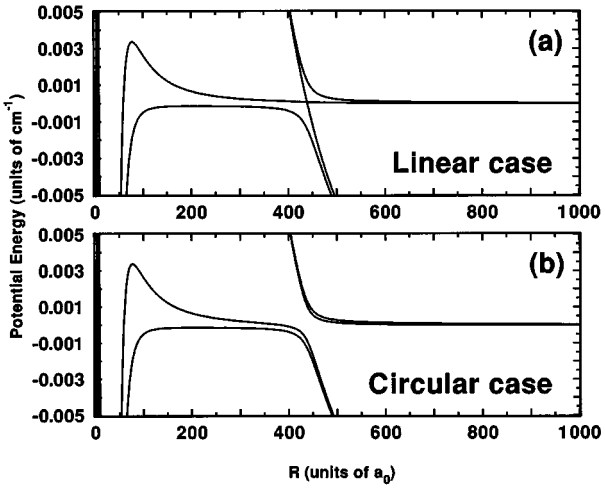

FIG. 7. Diagonalized potential curves in the region of the Condon point for $I=0.5$ W/cm^2 and up to $l=2$. In both cases, the ground state has $m_l=0$. (a) Linear polarization case showing that there is a crossing that is not avoided, meaning that only the P and R branches from the entrance d wave are allowed and the Q branch is absent. (b) Circular polarization case showing that all the curves avoid crossing, due to the fact that all three P, Q, and R branches from the entrance d wave are present.

are given in Fig. 7. In this region, the Hund's coupling case (a) basis of states is the most convenient to interpret the differences in the topologies of the linear and circular polarization cases. In the situations depicted in Fig. 7, an entrance d wave can absorb a photon and make a transition to an excited Π state. For linear polarization, there are only two branches that are allowed for such a transition: $J=2\to J'=1$ (P branch), and $J=2\to J'=3$ (R branch). For circular polarization, one more branch is allowed: $J=2\to J'=2$ (Q branch). These selection rules are the result of the matrix elements given by Eqs. (C4) and (C5), and are readily expressed by the conditions under which the Clebsch-Gordan coefficient $\langle 1,2,q,0|J,q\rangle$ is different from zero. The result of this difference between linear and circular polarizations is that there are more coupling matrix elements in the Hamiltonian for the circular case, resulting in more avoided crossings, than for the linear, and thus it is reasonable that the penetration to the inner region is more efficient for the linear case than for the circular. This dependence on polarization, due to multichannel effects, cannot be reproduced by a two-state Landau-Zener curve-crossing model, since such a theory can only account for the effects associated with only one branch (R branch). The presence of multiphoton processes is important here and multichannel curve crossings behave inherently differently from two-channel ones. In summary, it is the existence of the three branches to the repulsive excited states in the circular case and only two in the linear that implies a more efficient shielding in the circular case than in the linear. The results in Fig. 3 are in qualitative agreement with the Xe experiments [30], in which shielding measure approaches zero with increasing intensity much more slowly than the two-state models predict. However, Suominen *et al.* [30] have found that if a distribution of Rabi frequencies is assumed, then the two-state models can predict such qualitative variation with intensity. The as-

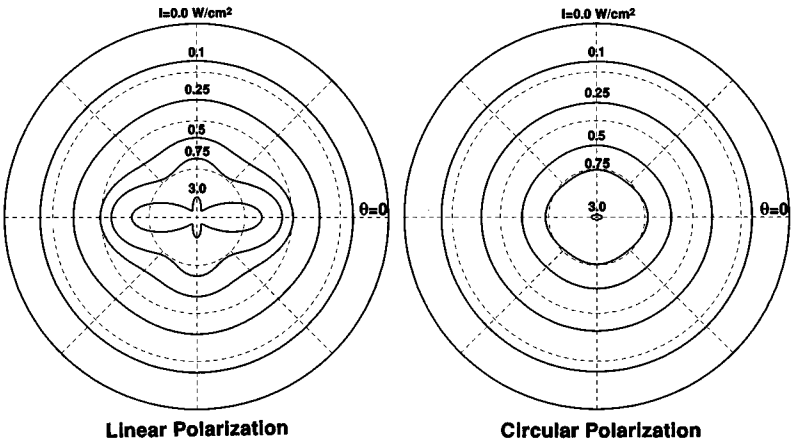

FIG. 8. Angular shielding measure for linearly and circularly polarized light. The numbers aligned vertically give the laser intensities in W/cm^2.

sumption of a distribution of Rabi frequencies does not have an obvious justification, but it could be useful in the context of complex systems including many hyperfine states.

F. Anisotropy of the optical shielding process

The significant contribution of the d wave in the linear case manifests itself as an anisotropic angular distribution of shielded collisions, regarding the angle between the entrance collision direction and the quantization axis. This effect can be calculated by integrating Eq. (24) over the final directions (θ,φ) only. The result is

$$\sigma_{1\to 5}(I,\vec{\theta_k},\vec{\varphi_k})=\frac{4\pi^2}{k_1^2}\sum_{l'=0}^{\infty}\sum_{m_l'=-l'}^{+l'}\left|\sum_{l=0}^{\infty}\sum_{m_l=-l}^{+l}\times Y_l^{m_l*}(\vec{\theta_k},\vec{\varphi_k})i^l T_{1,l,m_l}^{5,l',m_l'}(E)\right|^2. \quad (54)$$

Because at $I=0$ only the s wave penetrates to the inner region, $\sigma_{1\to 5}(I=0,\vec{\theta_k},\vec{\varphi_k})=\sigma_{1\to 5}(I=0)$ is isotropic and we define the angular shielding measure as

$$P_S(I,\vec{\theta_k},\vec{\varphi_k})\equiv\frac{\sigma_{1\to 5}(I,\vec{\theta_k},\vec{\varphi_k})}{\sigma_{1\to 5}(I=0)}. \quad (55)$$

It is worth noticing that, for linear polarization, the quantization axis is parallel to the electric field, and, for circular polarization, it is parallel to the direction of propagation of the light. Also, because the nonzero T matrix elements must satisfy $m_l'+q=m_l$, where m_l refers to the ground state and m_l' to the excited, the dependence on $\vec{\varphi_k}$ is eliminated from Eq. (54), and we need to consider $\vec{\theta_k}$ only. Figure 8 shows $P_S(I,\vec{\theta_k}\equiv\theta,\vec{\varphi_k}=0)$ for the linear and circular cases. It is evident from this figure how much the shielding by circularly polarized light is more efficient and isotropic than with linearly polarized light. In the linear case, the penetration into the inner region is most efficient if the atoms approach each other parallel to the direction of the light polarization vector. These predictions on shielding anisotropy could, in principle, be tested by cold atomic beam experiments, provided such investigations are realizable.

G. Excited-state production

A collision that is optically shielded can produce either two atoms in their ground states, or one atom in its ground state and the other in one of its excited states. The latter case generates fast atoms, for the repulsive excited state accelerates the separating atoms and causes them to gain kinetic energy. This kinetic energy increase can lead to trap loss and to a higher temperature of the atomic sample [22]. It is straightforward to obtain $K_{\rm ex}(I)\equiv K_{1\to 2}+K_{1\to 3}+K_{1\to 4}$ with the present formalism and the results are shown in Fig. 9. This figure also shows the Landau-Zener calculation given by the formula

$$K_{\rm ex}^{\rm LZ}(I)\equiv\sum_{l=0}^{\infty}(2l+1)\{2P_S^{\rm LZ}(I)[1-P_S^{\rm LZ}(I)]\}_{R_C(l)}, \quad (56)$$

where $P_S^{\rm LZ}(I)$ is the Landau-Zener probability of Eq. (49), the quantity within curly brackets is the probability of crossing the Condon point in the ground state without being excited on approach, followed by excitation on separation, plus the probability of being excited at the Condon point on approach, followed by deceleration in the excited state and crossing the Condon point again without being deexcited on separation; the factor $(2l+1)$ accounts for the degeneracy

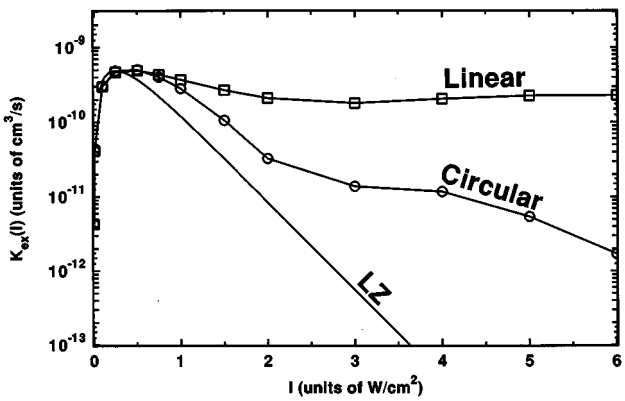

FIG. 9. Relaxation constant for producing one atom in its ground state and the other in one of its excited states. The linear and circular polarization cases are labeled with the words ''Linear'' and ''Circular,'' respectively. The Landau-Zener result is labeled ''LZ.''

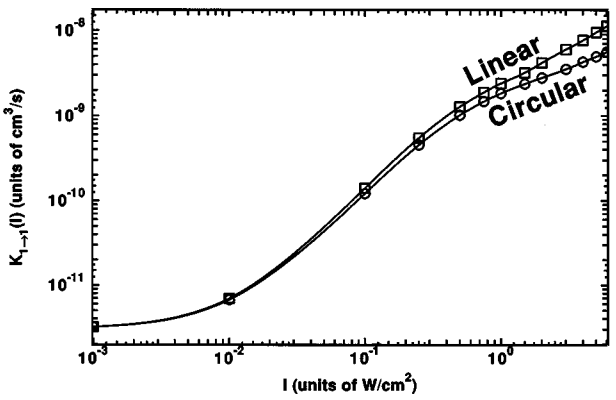

FIG. 10. Elastic scattering rate coefficient $K_{1\to1}(I)$ for linear and circular polarizations.

with respect to the m_l values, and the quantity within curly brackets is calculated at the Condon point $R_C(l)$, which is not the same for the potential curves of different partial waves. Both three-dimensional calculations show slower saturation than the R-branch Landau-Zener estimate, which implies that the three-dimensional situation contributes more excited-state production than predicted by two-state models. The linear case is predicted to be worse in terms of heat generation than the circular polarization case. This result is again a manifestation of the existence of more branches from the excited states back to the ground states in the circular case than in the linear. The only experimental test of excited-state production [22] was not far enough into the saturation regime to clearly test the validity of Landau-Zener models. The present calculations show that additional experiments are needed to establish the amount of excitation due to a blue-detuned laser.

H. Ground-state elastic-scattering

At long range, the ground state is the dressed state $|D_1\rangle Y_l^{m_l}(\theta,\varphi)$, whose potential is contaminated by the $1/R^3$ character of the excited-state dipole-dipole interaction. This mixing dramatically changes the threshold behavior of the ground-state scattering at moderate intensities as compared with the same elastic process in absence of the light [53]. As an illustration of this change in behavior, let us mention that Mott and Massey [54] show, on pages 44 and 45 of their book, that it is not possible to define a scattering length if the potential varies as $1/R^3$ at long range, but there is not such a restriction if the potential varies asymptotically as $1/R^6$, which is the case for $I=0$. The elastic rate coefficient $K_{1\to1}(I)$, as a function of intensity and polarization, is shown in Fig. 10. In both polarization cases, $K_{1\to1}(I)$ increases very fast with intensity and, at the highest intensity shown, 6 W/cm^2, there is a difference of less than one order of magnitude between the elastic rate coefficient in the linear and the circular cases. The elastic-scattering rate coefficient for the linear case is higher than for the circular at the highest intensities in Fig. 10 because the number of partial waves contributing appreciably to the linear cross section is greater than to the circular. For example, the cross section for the transition $(\beta=1,l=24,m_l=0)\rightarrow(\beta'=1,l'=24,m_l'=0)$ is about four times greater for the linear polarization case than for the circular.

The number of partial waves other than the s wave contributing to the elastic cross section is appreciable at modest intensities and this three-dimensional model predicts an accentuated increase in the elastic scattering of several orders of magnitude in a few W/cm^2 of increase in intensity. Furthermore, this large growth in the elastic cross section is achieved with substantial shielding of inelastic short-range processes and decreased production of excited-state atoms, as shown in Figs. 7 and 9, especially if circular polarization is used. It is also worth mentioning that even at relatively moderate intensities several partial waves are involved in the elastic-scattering and thus these rate coefficients do not exhibit purely s-wave Wigner threshold law behavior [55] in this temperature range. For example, we find that, at 2 W/cm^2 and an entrance kinetic energy corresponding to 0.1 nK, it is necessary to include at least up to $l=4$ in the calculation for converging the cross section to four significant figures. Ultimately, as the energy becomes low enough, only s waves will contribute to the elastic scattering. We will explore the many issues associated with elastic scattering, and modified scattering lengths, in a separate paper.

IV. SUMMARY

In this work we have shown that there are important effects in the three-dimensional, spinless model of optical suppression of ultracold-collision rates that cannot be predicted by one-dimensional, two-state models in the saturation regime. Despite the simplicity of these calculations, we have obtained results that are in qualitative agreement with recent experimental results. Specifically, the polarization sensitivity of the shielding in photoassociative ionization collision rates in a sodium magneto-optic trap has been unquestionably observed in a recent experiment [12], as qualitatively predicted by this simple model. The tool developed here is the generalization of the close-coupling theory to the three-dimensional, high-intensity-field situation. This approach is, indeed, pioneering into the realm of high-intensity light field effects on ultracold atomic collisions. In this regime, there is still much to be understood.

ACKNOWLEDGMENTS

J. W. and P. S. J. acknowledge support from the National Science Foundation, the Army Research Office, and the Office of Naval Research. R. N. acknowledges financial support from the Conselho Nacional de Desenvolvimento Científico e Tecnológico (CNPq) of Brazil.

APPENDIX A: BODY-FIXED TO SPACE-FIXED TRANSFORMATION

Given the body-fixed basis set of Eq. (5), the space-fixed electronic basis set is straightfowardly obtained by a rotation transformation:

$$|j,m_j\rangle=\sum_{\Lambda=-1}^{+1} D^{j*}_{m_j,\Lambda}(\varphi,\theta,0)|j,\Lambda\rangle, \qquad \text{(A1)}$$

where $D^{j*}_{m_j,\Lambda}(\varphi,\theta,0)$ are elements of the rotation matrix [37,56–58]. Using the property [52]

$$Y^{m_l}_l(\theta,\varphi)=\sqrt{\frac{2l+1}{4\pi}}D^{l*}_{m_l,0}(\varphi,\theta,0), \tag{A2}$$

and Eq. (A1), we can write

$$|j,m_j\rangle Y^{m_l}_l(\theta,\varphi)=\sqrt{\frac{2l+1}{4\pi}}\sum_{\Lambda=-1}^{+1}D^{j*}_{m_j,\Lambda}(\varphi,\theta,0)\times D^{l*}_{m_l,0}(\varphi,\theta,0)|j,\Lambda\rangle. \tag{A3}$$

From the expressions on page 58 of the book by Rose [56], we obtain

$$D^{j*}_{m_j,\Lambda}(\varphi,\theta,0)D^{l*}_{m_l,0}(\varphi,\theta,0)=\sum_{J=|l-j|}^{(l+j)}\sum_{M_J=-J}^{+J}\times\langle j,l,m_j,m_l|J,M_J\rangle\times\langle j,l,\Lambda,0|J,\Lambda\rangle D^{J*}_{M_J,\Lambda}(\varphi,\theta,0), \tag{A4}$$

where $\langle j,l,m_j,m_l|J,M_J\rangle$ and $\langle j,l,\Lambda,0|J,\Lambda\rangle$ are Clebsch-Gordan coefficients according to Messiah's notation [52]. Let us introduce the normalized symmetric top eigenfunctions [57]

$$\Theta^J_{M_J,\Lambda}(\theta,\varphi)\equiv\sqrt{\frac{2J+1}{4\pi}}D^{J*}_{M_J,\Lambda}(\varphi,\theta,0), \tag{A5}$$

where J is the total angular momentum quantum number ($\vec{J}\equiv\vec{l}+\vec{j}$) defined by the eigenvalue equation

$$(\vec{J}\cdot\vec{J})\Theta^J_{M_J,\Lambda}(\theta,\varphi)=\hbar^2J(J+1)\Theta^J_{M_J,\Lambda}(\theta,\varphi), \tag{A6}$$

with values $J=|l-j|,|l-j|+1,\ \ldots,\ l+j$. Thus Eqs. (A3)–(A5) give

$$|j,m_j\rangle Y^{m_l}_l(\theta,\varphi)=\sum_{J,M_J,\Lambda}\sqrt{\frac{2l+1}{2J+1}}\langle j,l,m_j,m_l|J,M_J\rangle\times\langle j,l,\Lambda,0|J,\Lambda\rangle|j,\Lambda,J,M_J\rangle, \tag{A7}$$

where we have defined

$$|j,\Lambda,J,M_J\rangle\equiv\Theta^J_{M_J,\Lambda}(\theta,\varphi)|j,\Lambda\rangle, \tag{A8}$$

and

$$\sum_{J,M_J,\Lambda}\equiv\sum_{J=|l-j|}^{(l+j)}\sum_{M_J=-J}^{+J}\sum_{\Lambda=-1}^{+1}. \tag{A9}$$

APPENDIX B: THE *S* MATRIX

Asymptotically, Eq. (19) gives

$$\lim_{R\to\infty}\left[\left(\frac{d^2}{dR^2}-\frac{l''(l''+1)}{R^2}\right)F^{\beta'',l'',m''_l}_{\beta',l',m'_l}(E,R)+\frac{2\mu}{\hbar^2}(E-E^\infty_{\beta''})F^{\beta'',l'',m''_l}_{\beta',l',m'_l}(E,R)\right]=0, \tag{B1}$$

where we have kept the centrifugal-potential term, $E^\infty_{\beta''}$ is the asymptotic value of H applied on $|D_{\beta''}\rangle Y^{l''}_{m''_l}(\theta,\varphi)$, and we have used

$$\vec{\nabla}^2_{\vec{R}}=\frac{1}{R}\frac{\partial^2}{\partial R^2}R-\frac{\vec{l}^{\,2}}{\hbar^2R^2}. \tag{B2}$$

In this work, we assume that the interaction between the two atoms decreases faster than R^{-2} asymptotically. Hence the general solution of the asymptotic radial Eq. (B10) is given by [54]

$$\lim_{R\to\infty}F^{\beta'',l'',m''_l}_{\beta',l',m'_l}(E,R)=A^{\beta'',l'',m''_l}_{\beta',l',m'_l}(k_{\beta''})j_l(k_{\beta''}R)+B^{\beta'',l'',m''_l}_{\beta',l',m'_l}(k_{\beta''})n_{l''}(k_{\beta''}R), \tag{B3}$$

where $A^{\beta'',l'',m''_l}_{\beta',l',m'_l}(k_{\beta''})$ and $B^{\beta'',l'',m''_l}_{\beta',l',m'_l}(k_{\beta''})$ are independent of R, $j_{l''}(k_{\beta''}R)$ and $n_{l''}(k_{\beta''}R)$ are the spherical Bessel and Neumann functions, respectively, and $k_{\beta''}$ is defined as

$$k_{\beta''}\equiv\sqrt{\frac{2\mu}{\hbar^2}(E-E^\infty_{\beta''})}. \tag{B4}$$

In this model, we assume $E>E^\infty_{\beta''}$ for all $\beta''=1,2,3,4,5$. Because the asymptotic forms of the Bessel and Neumann functions are given by [59]

$$\lim_{R\to\infty}j_{l''}(k_{\beta''}R)=\frac{\sin[k_{\beta''}R-(\pi/2)l'']}{k_{\beta''}R}\equiv\frac{e^{i[k_{\beta''}R-(\pi/2)l'']}-e^{-i[k_{\beta''}R-(\pi/2)l'']}}{2ik_{\beta''}R}, \tag{B5a}$$

$$\lim_{R\to\infty}n_{l''}(k_{\beta''}R)=-\frac{\cos[k_{\beta''}R-(\pi/2)l'']}{k_{\beta''}R}\equiv-\frac{e^{i[k_{\beta''}R-(\pi/2)l'']}+e^{-i[k_{\beta''}R-(\pi/2)l'']}}{2k_{\beta''}R}, \tag{B5b}$$

it follows that we can also express Eq. (B12) as

$$\lim_{R\to\infty} F^{\beta'',l'',m_l''}_{\beta',l',m_l'}(E,R) = C^{\beta'',l'',m_l''}_{\beta',l',m_l'}(k_{\beta''})\frac{e^{-i[k_{\beta''}R-(\pi/2)l'']}}{R} + D^{\beta'',l'',m_l''}_{\beta',l',m_l'}(k_{\beta''})\frac{e^{i[k_{\beta''}R-(\pi/2)l'']}}{R}, \tag{B6}$$

where $C^{\beta'',l'',m_l''}_{\beta',l',m_l'}(k_{\beta''})$ and $D^{\beta'',l'',m_l''}_{\beta',l',m_l'}(k_{\beta''})$ can be expressed in terms of the coefficients in Eq. (B3). Because [59]

$$e^{i\vec{k}_\beta\cdot\vec{R}} = \sum_{l=0}^{\infty}\sum_{m_l=-l}^{+l} 4\pi i^l Y_l^{m_l *}(\theta_{\vec{k}_\beta},\varphi_{\vec{k}_\beta}) Y_l^{m_l}(\theta,\varphi) j_l(k_\beta R), \tag{B7}$$

where $\vec{k}_\beta$ is a vector of magnitude k_β and polar angles $\theta_{\vec{k}_\beta}$ and $\varphi_{\vec{k}_\beta}$, we can form the linear combination

$$|\Psi_\beta(E,R\to\infty)\rangle \sim |D_\beta\rangle e^{i\vec{k}_\beta\cdot\vec{R}} + \sum_{\beta'=1}^{4}|D_{\beta'}\rangle\frac{e^{ik_{\beta'}R}}{R}\times\left(\frac{k_\beta}{k_{\beta'}}\right)^{1/2} f_\beta^{\beta'}(E,\theta_{\vec{k}_\beta},\varphi_{\vec{k}_\beta},\theta,\varphi), \tag{B8}$$

where $f_\beta^{\beta'}(E,\theta_{\vec{k}_\beta},\varphi_{\vec{k}_\beta},\theta,\varphi)$ is the scattering amplitude, and the sign ''$\sim$'' means that the left-hand side of Eq. (B8) is equal to its right-hand side up to a normalization factor. Equation (B8) is an asymptotic solution of Eq. (19) which includes the direction of the incident flux from the point of view of the atom at the origin. This dependence on $\theta_{\vec{k}_\beta}$ and $\varphi_{\vec{k}_\beta}$ does not appear in Eqs. (B3) and (B6). Thus let us introduce such a dependence by defining the superposition

$$|\overline{\Psi}_\beta(E,R)\rangle \equiv \sum_{l=0}^{\infty}\sum_{m_l=-l}^{+l} 4\pi i^l Y_l^{m_l *}(\theta_{\vec{k}_\beta},\varphi_{\vec{k}_\beta})|\Psi_{\beta,l,m_l}(E,R)\rangle. \tag{B9}$$

Assuming the normalization

$$\langle\Psi_{\beta,l,m_l}(E,R)|\Psi_{\beta',l',m_l'}(E',R)\rangle = \delta_{\beta,\beta'}\delta_{l,l'}\delta_{m_l,m_l'}\delta(E-E'), \tag{B10}$$

and imposing that the form of Eq. (B9) reduces to the form of Eq. (B8) in the limit $R\to\infty$ implies the asymptotic boundary condition of Eq. (21).

APPENDIX C: EXPLICIT EXPRESSION OF THE HAMILTONIAN MATRIX ELEMENTS

The total Hamiltonian can be written as $H=H_{\rm ni}+H_I$, where $H_{\rm ni}\equiv H_0+H_F$. Let us consider the matrix elements of H_I first. From Eq. (11), we obtain

$$\langle U_\gamma(R),l,m_l|H_I|U_{\gamma'}(R),l',m_l'\rangle = -i\left(\frac{2\pi\hbar\omega_L}{V_Q}\right)^{1/2}\langle U_\gamma(R),l,m_l|\vec{\mu}_M\cdot(\hat{\vec{\varepsilon}}_q a_q - \hat{\vec{\varepsilon}}_q^{\,*} a_q^\dagger)| \times U_{\gamma'}(R),l',m_l'\rangle. \tag{C1}$$

It follows from Eqs. (15) that the matrix element of Eq. (C1) is not zero only if either $\gamma=1$ and $\gamma'\neq 1,5$ or $\gamma'=1$ and $\gamma\neq 1,5$. Without loss of generality, let us consider the case for which $\gamma'=1$ and $\gamma\neq 1,5$. Therefore using Eqs. (13), (15), and (16), we obtain

$$\langle U_\gamma(R),l,m_l|H_I|U_1(R),l',m_l'\rangle = -i\left(\frac{2\pi}{c}I\right)^{\frac{1}{2}}\sum_{J,M_J,\Lambda}\sqrt{\frac{2l+1}{2J+1}}\langle 1,l,m_j(\gamma),m_l|J,M_J\rangle \times\langle 1,l,\Lambda,0|J,\Lambda\rangle\langle R,1,\Lambda,J,M_J|\vec{\mu}_M\cdot\hat{\vec{\varepsilon}}_q|R,0,0,l',m_l'\rangle. \tag{C2}$$

Since the polarization unit vector $\hat{\vec{\varepsilon}}_q$ is defined, for $q=0,\pm 1$, as

$$\hat{\vec{\varepsilon}}_0 \equiv \hat{\vec{z}},$$

$$\hat{\vec{\varepsilon}}_{\pm 1} \equiv \mp\frac{1}{\sqrt{2}}(\hat{\vec{x}}\pm i\hat{\vec{y}}), \tag{C3}$$

the quantity $\mu_q^{\rm SF}\equiv\vec{\mu}_M\cdot\hat{\vec{\varepsilon}}_q$ is the space-fixed q component of the spherical tensor operator of rank 1, $\vec{\mu}_M$. Thus using Eqs. (6), let us calculate

$$\begin{aligned}\langle R,j=1,\Lambda,J,M_J|\vec{\mu}_M\cdot\hat{\vec{\varepsilon}}_q|R,0,0,l',m_l'\rangle &\equiv \langle R,1,\Lambda,J,M_J|\mu_q^{\rm SF}|R,0,0,l',m_l'\rangle \\ &= \sum_{\kappa=-1}^{+1}\langle 1,{}^1X_u(R),\Lambda|\mu_\kappa^{\rm BF}(R)|0,{}^1\Sigma_g^+(R),0\rangle \\ &\quad\times\int_0^{2\pi}d\varphi\int_0^{\pi}\sin\theta d\theta\,\Theta^{J*}_{M_J,\Lambda}(\theta,\varphi)D^{1*}_{q,\kappa}(\varphi,\theta,0) \\ &\quad\times\Theta^{l'}_{m_l',0}(\theta,\varphi),\end{aligned} \tag{C4}$$

where $\mu_\kappa^{\rm BF}(R)$ is the body-fixed counterpart of $\mu_q^{\rm SF}$, ${}^1X_u(R)={}^1\Sigma_u(R)$ for $\Lambda=0$, and ${}^1X_u(R)={}^1\Pi_u(R)$ for $\Lambda=\pm 1$. Using Eq. (A5), we can show that [56]

$$\int_0^{2\pi}d\varphi\int_0^{\pi}\sin\theta d\theta\,\Theta^{J*}_{M_J,\Lambda}(\theta,\varphi)D^{1*}_{q,\kappa}(\varphi,\theta,0)\Theta^{l'}_{m_l',0}(\theta,\varphi) = \sqrt{\frac{2l'+1}{2J+1}}\langle 1,l',q,m_l'|J,M_J\rangle\langle 1,l',\kappa,0|J,\Lambda\rangle. \tag{C5}$$

From Eqs. (C2), (C4), and (C5), it follows that

$$\langle U_\gamma(R),l,m_l|H_I|U_1(R),l',m_l'\rangle$$
$$=-i\left(\frac{2\pi}{c}I\right)^{1/2}\sum_{J,M_J}\frac{\sqrt{(2l+1)(2l'+1)}}{2J+1}$$
$$\times\langle 1,l,m_j(\gamma),m_l|J,M_J\rangle\langle 1,l',q,m_l'|J,M_J\rangle$$
$$\times\sum_{\Lambda=-1}^{+1}\langle 1,l,\Lambda,0|J,\Lambda\rangle\langle 1,l',\Lambda,0|J,\Lambda\rangle$$
$$\times\langle 1,{}^1X_u(R),\Lambda|\mu_\Lambda^{\rm BF}(R)|0,{}^1\Sigma_g^+(R),\Lambda'=0\rangle. \quad \text{(C6)}$$

Because we are considering optical collisions, in which the electromagnetic coupling is not zero asymptotically, we will neglect the R-dependent part of the matrix element $\langle 1,{}^1X_u(R),\Lambda|\mu_\Lambda^{\rm BF}(R)|0,{}^1\Sigma_g^+(R)\rangle$ [33,34]. Thus we approximate Eq. (C6) by

$$\langle U_\gamma(R),l,m_l|H_I|U_1(R),l',m_l'\rangle$$
$$\approx -i\left(\frac{2\pi}{c}I\right)^{1/2}\sum_{J,M_J}\frac{\sqrt{(2l+1)(2l'+1)}}{2J+1}$$
$$\times\langle 1,l,m_j(\gamma),m_l|J,M_J\rangle\langle 1,l',q,m_l'|J,M_J\rangle$$
$$\times\sum_{\Lambda=-1}^{+1}\langle 1,l,\Lambda,0|J,\Lambda\rangle\langle 1,l',\Lambda,0|J,\Lambda\rangle$$
$$\times\langle 1,\Lambda|\mu_\Lambda^{\rm BF}(\infty)|0,\Lambda'=0\rangle, \quad \text{(C7)}$$

where $\mu_\Lambda^{\rm BF}(\infty)\equiv\mu_\Lambda^{\rm BF}(R\to\infty)$ and the states $|j,\Lambda\rangle$ are defined by Eq. (5). From Eq. (A1) and the orthonormality relation [56]

$$\sum_m D^{j*}_{m,\lambda}(\varphi,\theta,0)D^j_{m,\kappa}(\varphi,\theta,0)=\delta_{\lambda,\kappa}, \quad \text{(C8)}$$

we obtain

$$\langle 1,\Lambda|\mu_\Lambda^{\rm BF}(R\to\infty)|0,\Lambda'=0\rangle$$
$$=\frac{1}{\sqrt{3}}\sum_{m_j}\sum_{m_j'}D^{j*}_{m_j,\Lambda}(\varphi,\theta,0)D^j_{m_j',\Lambda}(\varphi,\theta,0)$$
$$\times\langle j=1\|\mu^{\rm SF}\|j''=0\rangle\langle 0,1,0,m_j'|1,m_j\rangle$$
$$=\frac{1}{\sqrt{3}}\langle j=1\|\mu^{\rm SF}\|j''=0\rangle, \quad \text{(C9)}$$

where we have used Wigner-Eckart theorem [52] and $\langle j=1\|\mu^{\rm SF}\|j''=0\rangle$ is the relevant reduced matrix element of $\vec{\mu}_M$. From Eqs. (C7) and (C9), and the properties of the Clebsch-Gordan coefficients [52], we obtain

$$\langle U_\gamma(R),l,m_l|H_I|U_1(R),l',m_l'\rangle$$
$$\approx -i\left(\frac{2\pi}{3c}I\right)^{1/2}\langle j=1\|\mu^{\rm SF}\|j''=0\rangle\delta_{m_j(\gamma),q}\delta_{l,l'}\delta_{m_l,m_l'}. \quad \text{(C10)}$$

Applying Wigner-Eckart theorem on Eq. (12) allows us to express Eq. (C10) in terms of the Rabi frequency Ω:

$$\langle U_\gamma(R),l,m_l|H_I|U_1(R),l',m_l'\rangle\approx\hbar\Omega\,\delta_{m_j(\gamma),q}\delta_{l,l'}\delta_{m_l,m_l'}. \quad \text{(C11)}$$

To relate the molecular Rabi frequency Ω with the atomic Rabi frequency Ω^A, we use Eqs. (27) and (28). Thus we get

$$\Omega=\sqrt{2}\Omega^A. \quad \text{(C12)}$$

The numerical value of Ω^A we take in this work is based on the $3s\to 3p$ transition of the sodium atom (neglecting fine and hyperfine structures). Thus for an intensity I given in W/cm^2, we use the formula

$$\frac{\Omega^A}{2\pi c}\approx 1.479\,66\times 10^{-3}\sqrt{I(W/cm^2)}\ \text{cm}^{-1}. \quad \text{(C13)}$$

The noninteracting Hamiltonian $H_{\rm ni}$ can be written as a sum of three terms:

$$H_{\rm ni}=-\frac{\hbar^2}{2\mu}\frac{1}{R}\frac{\partial^2}{\partial R^2}R+\frac{\vec{l}^{\,2}}{2\mu R^2}+W(R). \quad \text{(C14)}$$

Thus let us now consider the matrix elements of $W(R)$ for the cases in which $\gamma,\gamma'\neq 5$:

$$\langle U_\gamma(R),l,m_l|W(R)|U_{\gamma'}(R),l',m_l'\rangle$$
$$=\delta_{j(\gamma),j(\gamma')}\sum_{J,M_J,\Lambda}\frac{\sqrt{(2l+1)(2l'+1)}}{2J+1}$$
$$\times\langle j(\gamma),l,m_j(\gamma),m_l|J,M_J\rangle$$
$$\times\langle j(\gamma'),l',m_j(\gamma'),m_l'|J,M_J\rangle\langle j(\gamma),l,\Lambda,0|J,\Lambda\rangle$$
$$\times\langle j(\gamma'),l',\Lambda,0|J,\Lambda\rangle W^{j(\gamma)}_{|\Lambda|}(R), \quad \text{(C15)}$$

where we have defined $j(\gamma=1)\equiv 0$, and $j(\gamma=2,3,4)\equiv 1$. From Eq. (C15), it follows that

$$\langle U_1(R),l,m_l|W(R)|U_1(R),l',m_l'\rangle=\delta_{l,l'}\delta_{m_l,m_l'}W_0^0(R), \quad \text{(C16)}$$

$$\langle U_1(R),l,m_l|W(R)|U_{\gamma'\neq 1,5}(R),l',m_l'\rangle$$
$$=\langle U_{\gamma\neq 1,5}(R),l,m_l|W(R)|U_1(R),l',m_l'\rangle$$
$$=0, \quad \text{(C17)}$$

$$\langle U_{\gamma\neq 1,5}(R),l,m_l|W(R)|U_{\gamma'\neq 1,5}(R),l',m_l'\rangle$$
$$=\sum_{J,M_J}\frac{\sqrt{(2l+1)(2l'+1)}}{2J+1}\langle 1,l,m_j(\gamma),m_l|J,M_J\rangle$$
$$\times\langle 1,l',m_j(\gamma'),m_l'|J,M_J\rangle\sum_{\Lambda=-1}^{+1}\langle 1,l,\Lambda,0|J,\Lambda\rangle$$
$$\times\langle 1,l',\Lambda,0|J,\Lambda\rangle W^1_{|\Lambda|}(R). \quad \text{(C18)}$$

Since

$$\sum_{\Lambda=-1}^{+1}\langle 1,l,\Lambda,0|J,\Lambda\rangle\langle 1,l',\Lambda,0|J,\Lambda\rangle W^1_{|\Lambda|}(R)$$
$$=\langle 1,l,0,0|J,0\rangle\langle 1,l',0,0|J,0\rangle W^1_0(R)$$
$$+[1+(-1)^{l+l'}]\langle 1,l,1,0|J,1\rangle\langle 1,l',1,0|J,1\rangle W^1_1(R), \tag{C19}$$

we conclude that

$$\langle U_{\gamma\neq 1,5}(R),l,m_l|W(R)|U_{\gamma'\neq 1,5}(R),l',m_l'\rangle=0$$

unless $l'=l,l\pm 2$. For the artificial state, we take

$$\langle U_{\gamma\neq 1,5}(R),l,m_l|W(R)|U_5(R),l',m_l'\rangle$$
$$=\langle U_5(R),l,m_l|W(R)|U_{\gamma'\neq 1,5}(R),l',m_l'\rangle$$
$$=0, \tag{C20}$$

$$\langle U_1(R),l,m_l|W(R)|U_5(R),l',m_l'\rangle$$
$$=\langle U_5(R),l,m_l|W(R)|U_1(R),l',m_l'\rangle$$
$$=\delta_{l,l'}\delta_{m_l,m_l'}D_A(R), \tag{C21}$$

$$\langle U_5(R),l,m_l|W(R)|U_5(R),l',m_l'\rangle=\delta_{l,l'}\delta_{m_l,m_l'}W_A(R). \tag{C22}$$

The centrifugal part of $H_{\rm ni}$ gives rise to the following matrix elements:

$$\left\langle U_\gamma(R),l,m_l\left|\frac{\vec{l}^{\,2}}{2\mu R^2}\right|U_{\gamma'}(R),l',m_l'\right\rangle$$
$$=\delta_{\gamma,\gamma'}\delta_{l,l'}\delta_{m_l,m_l'}\frac{\hbar^2 l(l+1)}{2\mu R^2}$$
$$-\left\langle U_\gamma(R),l,m_l\left|\frac{\vec{l}^{\,2}-\hbar^2 l(l+1)}{2\mu R^2}\right|U_{\gamma'}(R),l',m_l'\right\rangle, \tag{C23}$$

where the last equality follows from the fact that the matrix elements in Eq. (C23) do not involve an integration over R in their definition. In this model calculation, we assume that the term $-\langle U_\gamma(R),l,m_l|[\vec{l}^{\,2}-\hbar^2 l(l+1)]/2\mu R^2|U_{\gamma'}(R),l',m_l'\rangle$ is negligible and write Eq. (C23) as

$$\left\langle U_\gamma(R),l,m_l\left|\frac{\vec{l}^{\,2}}{2\mu R^2}\right|U_{\gamma'}(R),l',m_l'\right\rangle$$
$$\approx\delta_{\gamma,\gamma'}\delta_{l,l'}\delta_{m_l,m_l'}\frac{\hbar^2 l(l+1)}{2\mu R^2}. \tag{C24}$$

Here we assume that the Born-Oppenheimer approximation [35] is valid, as already discussed in Sec. II. This assumption is further yet justified because the excitation process is the one dynamical effect that we are investigating and it occurs at about $400a_0$, a region where the potentials are already given by their asymptotic behaviors. Therefor the term neglected in Eq. (C24) depends on R as R^{-n_∞}, where $n_\infty>2$, implying that the centrifugal R^{-2} term is the leading one at the dynamically relevant region. Of course, an exact theory would require the correct expression, Eq. (C23), at very short range, but we have already defined the process we want to investigate: the suppression of production of two atoms in the artificial state, which can be studied carefully without the complications of the neglected term in Eq. (C24).

The radial term of $H_{\rm ni}$ gives the following matrix elements:

$$\left\langle U_\gamma(R),l,m_l\left|-\frac{\hbar^2}{2\mu}\frac{1}{R}\frac{\partial^2}{\partial R^2}R\right|U_{\gamma'}(R),l',m_l'\right\rangle$$
$$=-\frac{\hbar^2}{2\mu}\delta_{\gamma,\gamma'}\delta_{l,l'}\delta_{m_l,m_l'}\frac{1}{R}\frac{\partial^2}{\partial R^2}R$$
$$-\frac{\hbar^2}{\mu}\left\langle U_\gamma(R),l,m_l|\frac{\partial|U_{\gamma'}(R),l',m_l'\rangle}{\partial R}\right\rangle\left(\frac{1}{R}+\frac{\partial}{\partial R}\right)$$
$$-\frac{\hbar^2}{2\mu}\left\langle U_\gamma(R),l,m_l|\frac{\partial^2|U_{\gamma'}(R),l',m_l'\rangle}{\partial R^2}\right\rangle. \tag{C25}$$

We assume that the radial Born-Oppenheimer terms are negligible and write Eq. (C25) as

$$\left\langle U_\gamma(R),l,m_l\left|-\frac{\hbar^2}{2\mu}\frac{1}{R}\frac{\partial^2}{\partial R^2}R\right|U_{\gamma'}(R),l',m_l'\right\rangle$$
$$=-\frac{\hbar^2}{2\mu}\delta_{\gamma,\gamma'}\delta_{l,l'}\delta_{m_l,m_l'}\frac{1}{R}\frac{\partial^2}{\partial R^2}R. \tag{C26}$$

Again, the justification we have given for Eq. (C24) also applies here for Eq. (C26), since extra Born-Oppenheimer terms that are not important in the excitation region only complicate the problem without clarifying the issue, and we are building a model calculation that is only intended to reproduce experimental results in a qualitative manner. The reader interested in how to estimate the long-range values of the Born-Oppenheimer terms can find a very insightful example in Ref. [40].

Now we have all the necessary quantities that enter Eq. (19), which is first of all written in terms of the basis states of Eqs. (14) and (30) by using Eq. (20). The Hamiltonian in matrix form, Eq. (38), is then written in terms of the undressed basis states through Eqs. (29) and (40). All the different matrix elements in the undressed basis are given by Eqs. (C11)–(C26).

[1] M. H. Anderson, J. R. Ensher, M. R. Matthews, C. E. Wieman, and E. A. Cornell, Science **269**, 198 (1995).
[2] C. C. Bradley, C. A. Sackett, J. J. Tollett, and H. G. Hulet, Phys. Rev. Lett. **75**, 1687 (1995).
[3] K. B. Davis, M.-O. Mewes, M. R. Andrews, N. J. van Druten, D. S. Durfee, D. M. Kurn, and W. Ketterle, Phys. Rev. Lett. **75**, 3969 (1995).
[4] J. Weiner, Adv. At. Mol. Opt. Phys. **35**, 45 (1995).

[5] L. E. Reichl, *A Modern Course in Statistical Physics* (University of Texas Press, Austin, 1980).
[6] V. Bagnato and D. Kleppner, Phys. Rev. A **44**, 7439 (1991).
[7] P. S. Julienne, A. M. Smith, and K. Burnett, in *Advances in Atomic, Molecular, and Optical Physics*, edited by D. R. Bates and B. Bederson (Academic Press, San Diego, CA, 1993), Vol. 30, p. 141.
[8] D. Sesko, T. Walker, C. Monroe, A. Gallagher, and C. Wieman, Phys. Rev. Lett. **63**, 961 (1989).
[9] A. Gallagher and D. E. Pritchard, Phys. Rev. Lett. **63**, 957 (1989).
[10] P. S. Julienne and J. Vigué, Phys. Rev. A **44**, 4464 (1991).
[11] C. D. Wallace, T. P. Dinneen, K.-Y. N. Tan, T. T. Grove, and P. L. Gould, Phys. Rev. Lett. **69**, 897 (1992).
[12] S. C. Zilio, L. Marcassa, S. Muniz, R. Horowicz, V. Bagnato, R. Napolitano, J. Weiner, and P. S. Julienne, Phys. Rev. Lett. **76**, 2033 (1996).
[13] D. Hoffman, P. Feng, R. Williamson, and T. Walker, Phys. Rev. Lett. **69**, 753 (1992).
[14] L. Marcassa, V. Bagnato, Y. Wang, C. Tsao, J. Weiner, O. Dulieu, Y. B. Band, and P. S. Julienne, Phys. Rev. A **47**, R4563 (1993).
[15] J. Kawanake, K. Shimizu, H. Tanaka, and F. Shimizu, Phys. Rev. A **48**, R883 (1993).
[16] N. W. M. Ritchie, E. R. I. Abraham, Y. X. Xiao, C. C. Bradley, R. G. Hulet, and P. S. Julienne (unpublished).
[17] J. D. Miller, R. A. Cline, and D. J. Heinzen, Phys. Rev. Lett. **71**, 2204 (1993).
[18] R. A. Cline, J. D. Miller, and D. J. Heinzen, Phys. Rev. Lett. **73**, 632 (1994).
[19] H. T. C. Stoof, J. M. V. A. Koelman, and B. J. Verhaar, Phys. Rev. B **38**, 4688 (1988).
[20] E. Tiesinga, A. J. Moerdijk, B. J. Verhaar, and H. T. C. Stoof, Phys. Rev. A **46**, R1167 (1992).
[21] B. Verhaar, K. Gibble, and S. Chu, Phys. Rev. A **48**, R3429 (1993).
[22] S. Bali, D. Hoffmann, and T. Walker, Europhys. Lett. **27**, 273 (1994).
[23] L. Marcassa, S. Muniz, E. de Queiroz, S. Zilio, V. Bagnato, J. Weiner, P. S. Julienne, and K.-A. Suominen, Phys. Rev. Lett. **73**, 1911 (1994).
[24] L. Marcassa, R. Horowicz, S. Zilio, V. Bagnato, and J. Weiner, Phys. Rev. A **52**, R913 (1995).
[25] M. Walhout, U. Sterr, C. Orzel, M. Hoogerland, and S. L. Rolston, Phys. Rev. Lett. **74**, 506 (1995).
[26] H. Katori and F. Shimizu, Phys. Rev. Lett. **73**, 2555 (1994).
[27] C. D. Wallace, V. Sanchez-Villicana, T. P. Dinneen, and P. L. Gould, Phys. Rev. Lett. **74**, 1087 (1995).
[28] K.-A. Suominen, M. J. Holland, K. Burnett, and P. S. Julienne, Phys. Rev. A **51**, 1446 (1995).
[29] C. J. Williams and P. S. Julienne, J. Chem. Phys. **101**, 2634 (1994).
[30] K.-A. Suominen, K. Burnett, P. S. Julienne, M. Walhout, U. Sterr, C. Orzel, M. Hoogerland, and S. L. Rolston, Phys. Rev. A **53**, 1678 (1996).
[31] C. J. Williams, E. Tiesinga, and P. S. Julienne (unpublished).
[32] P. S. Julienne and F. H. Mies, Phys. Rev. A **25**, 3399 (1982).
[33] P. S. Julienne and F. H. Mies, Phys. Rev. A **30**, 831 (1984).
[34] P. S. Julienne and F. H. Mies, Phys. Rev. A **34**, 3792 (1986).
[35] M. Born and J. R. Oppenheimer, Ann. Phys. (Leipzig) **84**, 457 (1927).
[36] G. Herzberg, *Molecular Spectra and Molecular Structure. Volume I - Spectra of Diatomic Molecules* 2nd ed. (Van Nostrand, New York, 1950).
[37] R. N. Zare, A. L. Schmeltekopf, W. J. Harrop, and D. L. Albritton, J. Mol. Spectrosc. **46**, 37 (1973).
[38] Edwin A. Power, J. Chem. Phys. **46**, 4297 (1967).
[39] C. Cohen-Tannoudji, J. Dupont-Roc, and G. Grynberg, *Interaction Processes between Photons and Atoms* (Wiley, New York, 1992).
[40] F. H. Mies, Phys. Rev. A **7**, 942 (1973).
[41] F. H. Mies, in *Theoretical Chemistry: Advances and Perspectives*, edited by D. Henderson (Academic, New York, 1981), pp. 127–198.
[42] F. H. Mies, Mol. Phys. **14**, 953 (1980).
[43] Paul Roman, *Advanced Quantum Theory. An Outline of The Fundamental Ideas* (Addison-Wesley, Reading, MA, 1965).
[44] M. P. I. Manders, W. Boom, H. C. W. Beijerinck, and B. J. Verhaar, Phys. Rev. A **39**, 5021 (1989).
[45] R. W. Heather and P. S. Julienne, Phys. Rev. A **47**, 1887 (1993).
[46] H. R. Thorsheim, J. Weiner, and P. S. Julienne, Phys. Rev. Lett. **58**, 2420 (1987).
[47] B. Bussery and M. Aubert-Frecon, J. Chem. Phys. **82**, 3224 (1985).
[48] S. Magnier, Ph. Milli, O. Dulieu, and F. Masnou-Seeuws, J. Chem. Phys. **98**, 7113 (1993).
[49] William J. Meath, J. Chem. Phys. **48**, 227 (1968).
[50] R. Gordon, J. Chem. Phys. **51**, 14 (1969).
[51] R. Gordon, Methods Comput. Phys. **10**, 81 (1971).
[52] A. Messiah, *Quantum Mechanics* (North-Holland, Amsterdam, 1965).
[53] P. S. Julienne, Phys. Rev. Lett. **61**, 698 (1988).
[54] N. F. Mott and H. S. W. Massey, *The Theory Of Atomic Collisions*, 3rd ed. (Oxford, London, 1965).
[55] R. Napolitano, J. Weiner, C. J. Williams, and P. S. Julienne, Phys. Rev. Lett. **73**, 1352 (1994).
[56] M. E. Rose, *Elementary Theory of Angular Momentum* (Wiley, New York, 1957).
[57] D. M. Brink and G. R. Satchler, *Angular Momentum* (Oxford University Press, London, 1962).
[58] A. A. Wolf, Am. J. Phys. **37**, 531 (1969).
[59] George Arfken, *Mathematical Methods for Physicists* (Academic Press, San Diego, CA, 1985).